

# **EXPERIMENTAL AND NUMERICAL STUDIES OF DUCTILE REGIME MACHINING OF SILICON CARBIDE AND SILICON NITRIDE**

Ravishankar Mariayyah  
Department of Mechanical Engineering  
University of North Carolina at Charlotte

Advisors: Dr. Harish P. Cherukuri and Dr. John A. Patten

# Outline

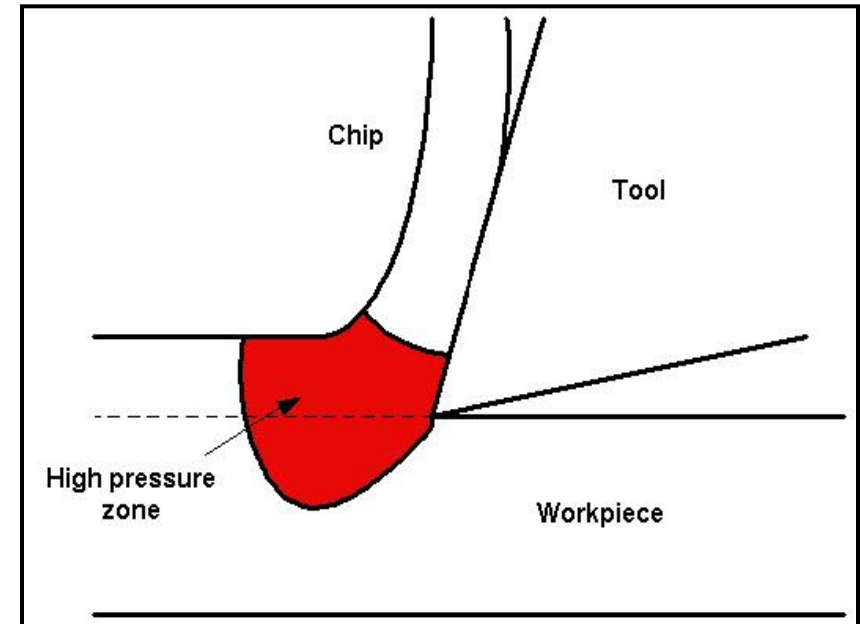
- Introduction -Ductile regime machining and HPPT.
- Experimental work.
- Numerical simulations.
- Conclusions and future work.

# Ductile regime machining

- Under certain controlled conditions, it is possible to machine brittle materials in 'ductile regime' so that material removal is by plastic deformation, leaving a damage free surface.
- Experiments such as nano-indentation and scratching of Silicon and Germanium indicate that ductile behavior is a pressure-induced phenomenon.
- Brittle-ductile phase transition takes place when the hydrostatic pressure during loading approaches the hardness values.
- Since this transition takes place at high hydrostatic pressures they are otherwise called as High Pressure Phase Transformations (HPPT).

# Ductile regime machining - continued

- A high-pressure zone is present at the cutting tool and workpiece interface.
- Workpiece material passing through this zone undergoes brittle-ductile transition.
- The extent of this zone depends on rake angle, depth of cut, cutting edge radius and feed.



Courtesy: Ronnie Fesperman & Satya kumar Ajarappu

# Examples of HPPT

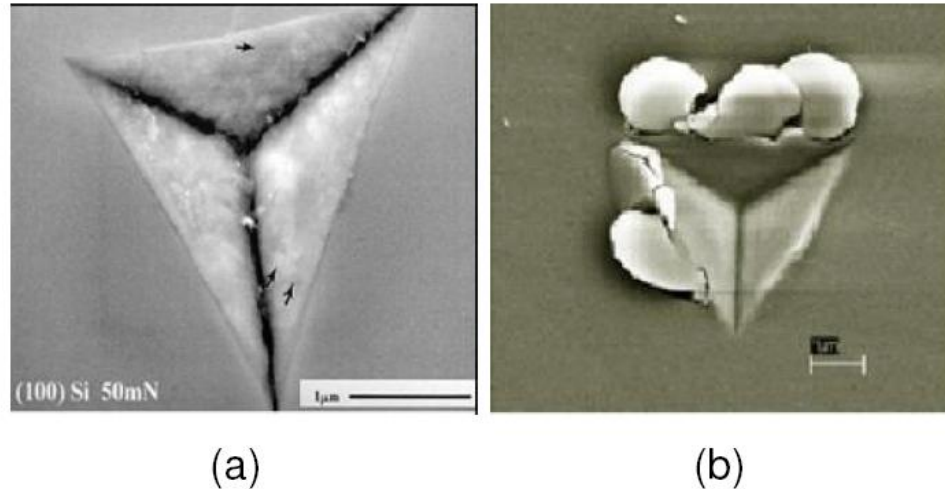
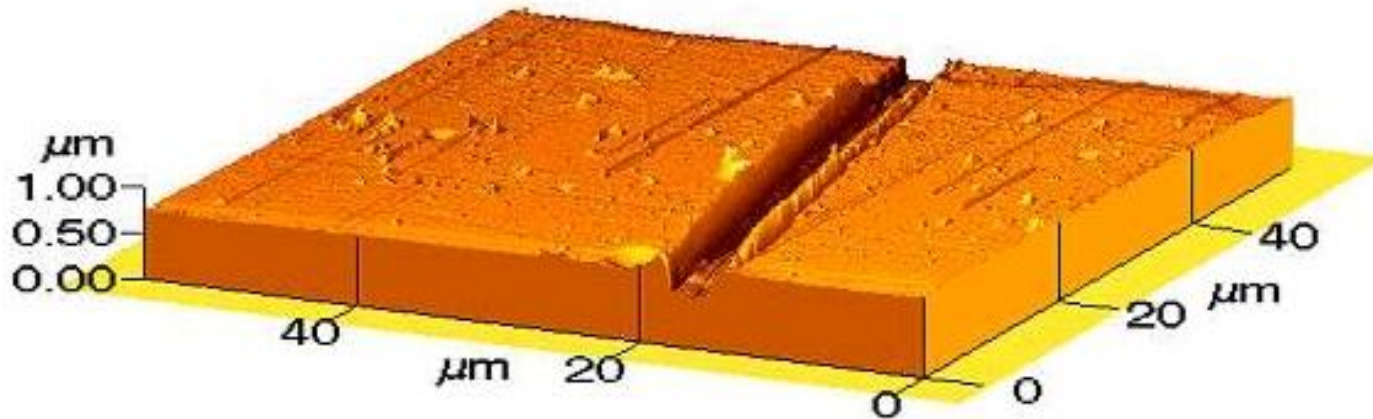


Figure: SEM image of the indentation of (a) Silicon and (b) SiC

Courtesy: Jennifer et al., UV Raman Scattering Analysis of Indented and Machined 6H-SiC and  $\beta$ - $Si_3N_4$  Surfaces, Material Research Gateway, Mater. Res. Soc. Symp. Proc. vol.843, 2005.

# Examples of HPPT – continued..



Atomic Force Microscopy (AFM) image of silicon

Courtesy: John. A. Patten, Ductile response of silicon carbide, Evidence of High Pressure Phase Transformation? HPPT 2005 Workshop, University of Tennessee, Knoxville

# Focus of the thesis work

## Experimental studies

1. To identify the conditions under which ductile regime machining is possible when silicon carbide and silicon nitride materials are machined using Single Point Diamond Turning.
2. To identify the mechanisms of toolwear for various cutting conditions and tool geometry during edge machining for these two materials.

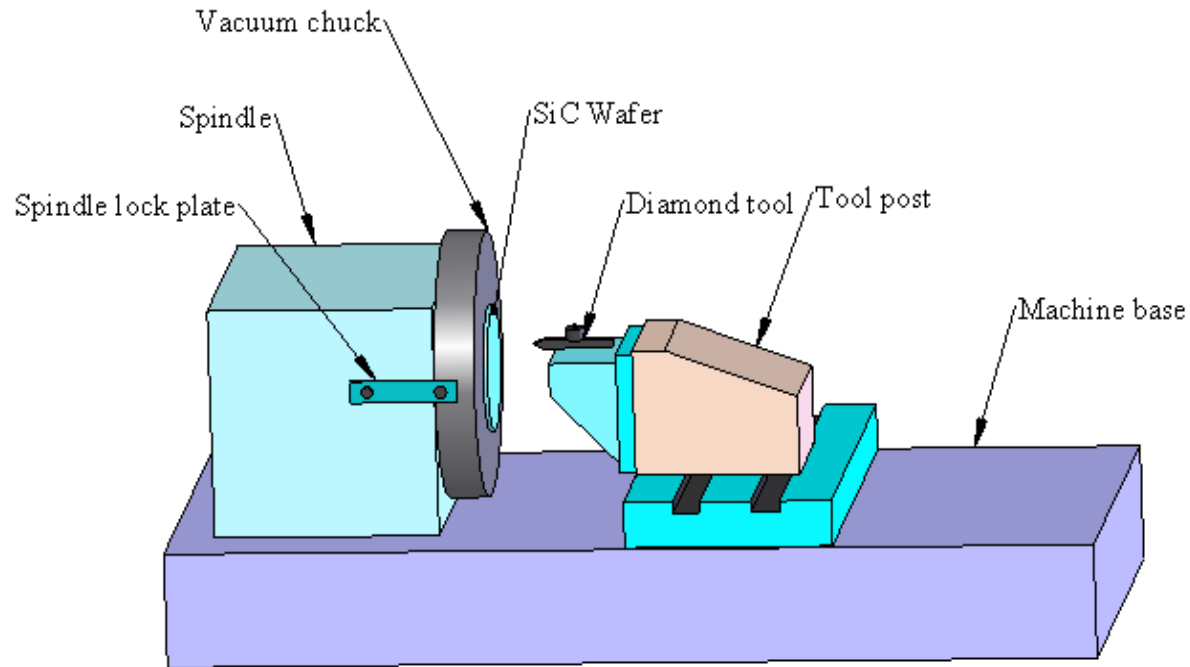
## Numerical studies

1. To study the possibility of hydrostatic pressure and shear stress induced phase transformation during machining of silicon carbide by a single point diamond tool by considering the initial stages of machining prior to material separation as a nanoindentation problem.
2. To develop a finite element model for orthogonal machining of silicon carbide by accommodating pressure dependent phase transformations and volume change in the material behavior. 7

# Overview of experimental work

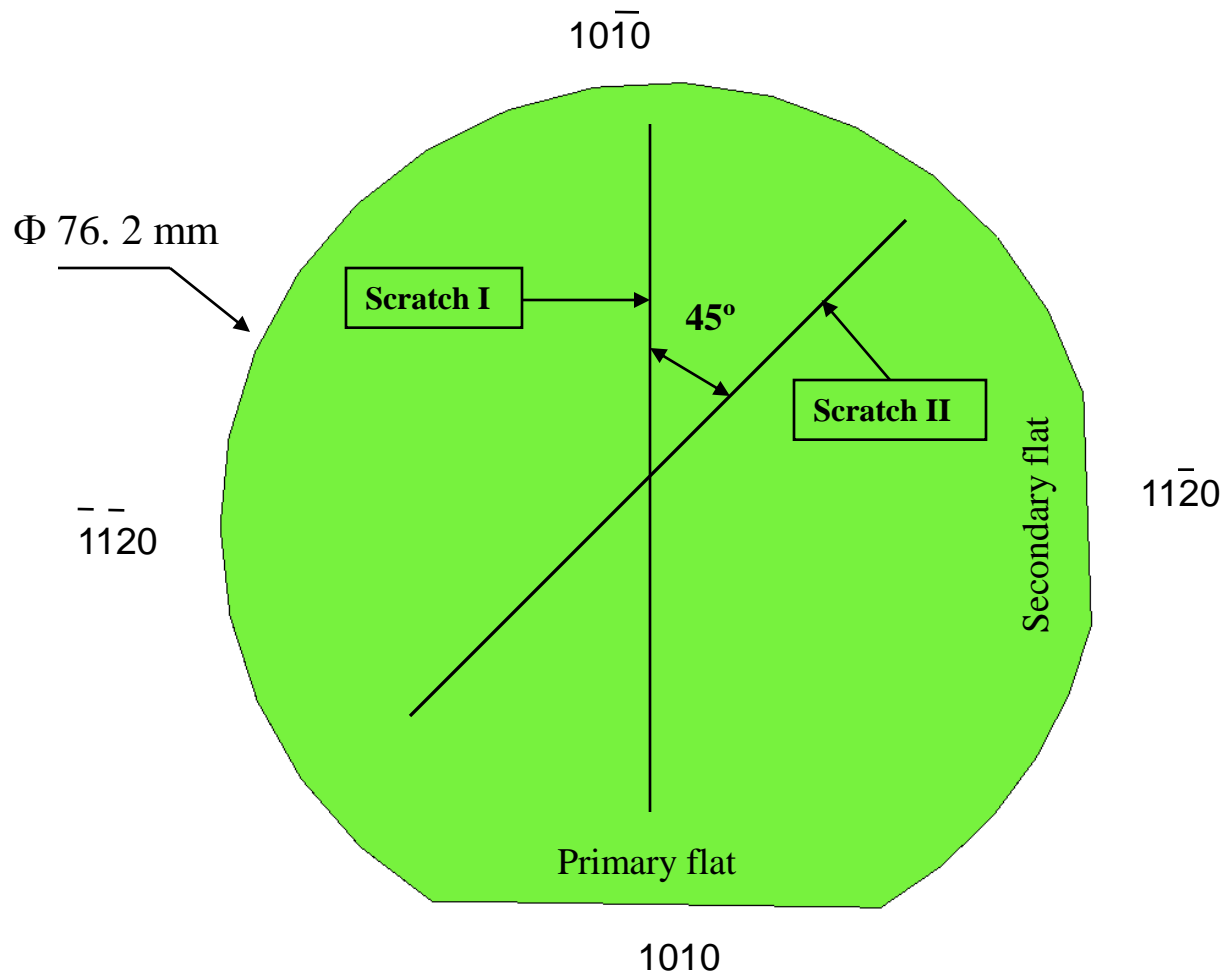
- Scratch tests on single crystal SiC.
- Edge machining tests on single crystal SiC.
- Tool wear studies of a silicon nitride workpiece during SPDT.
- Si Plate machining (not include here).
- Kolsky bar tests (not included here).

# Scratch tests on single crystal SiC

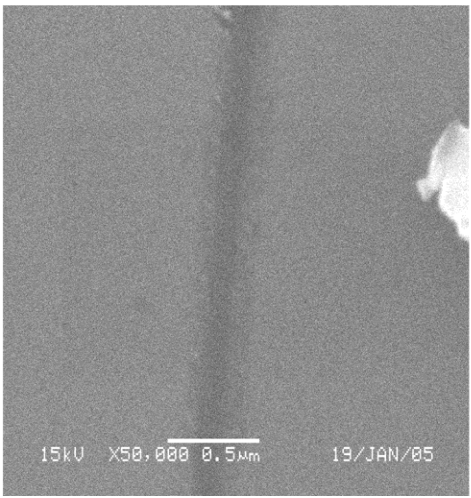


Experimental Setup – Scratch test

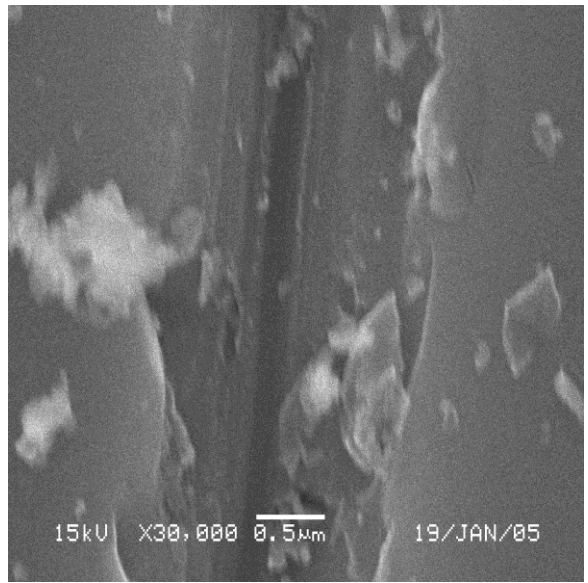
# Scratches in the 4-H SiC Wafer



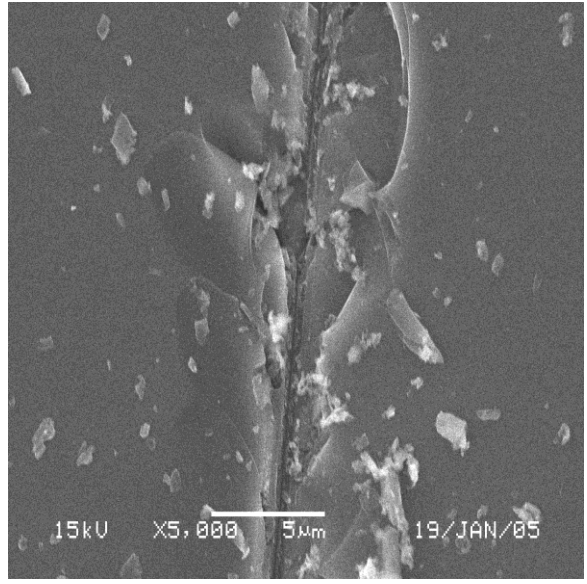
# SEM images



(a)



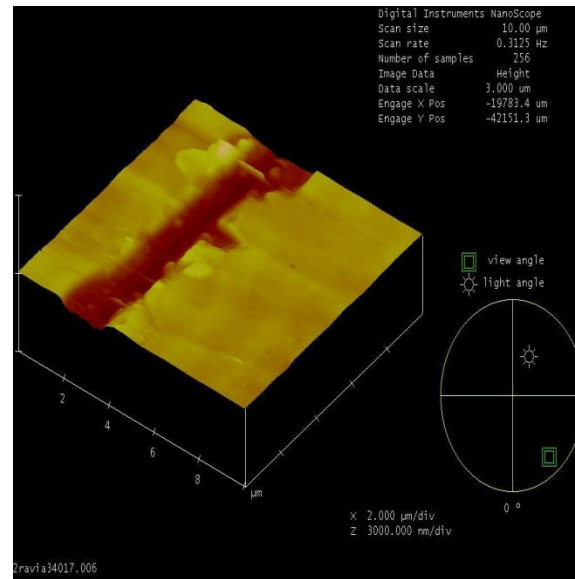
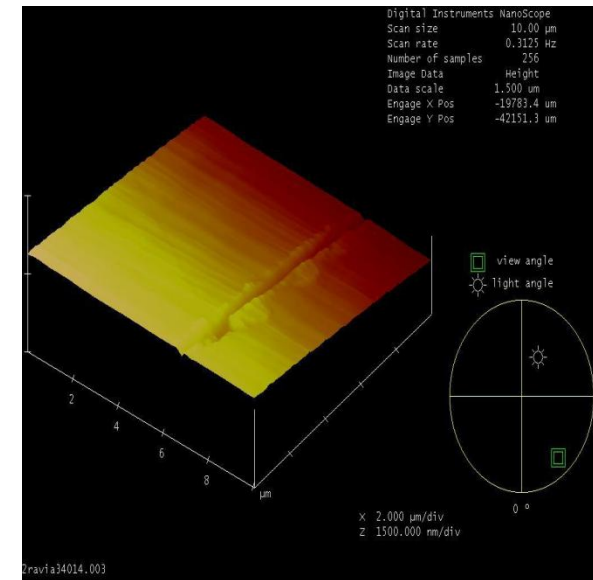
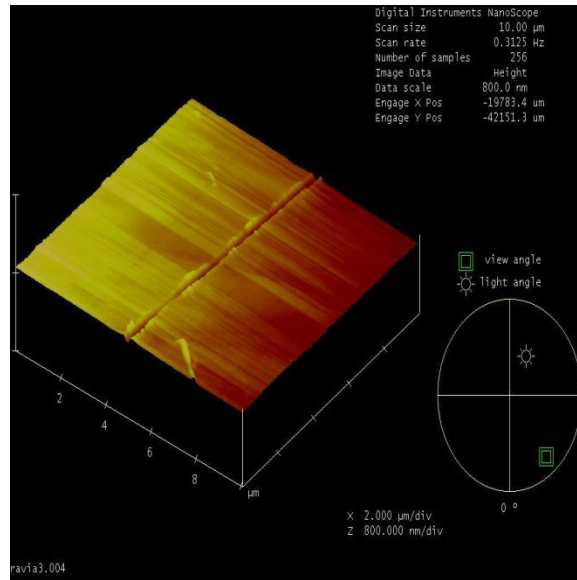
(b)



(c)

10/25/2007 SEM image of scratch I in (a) ductile, (b) transition and (c) brittle region

# AFM images



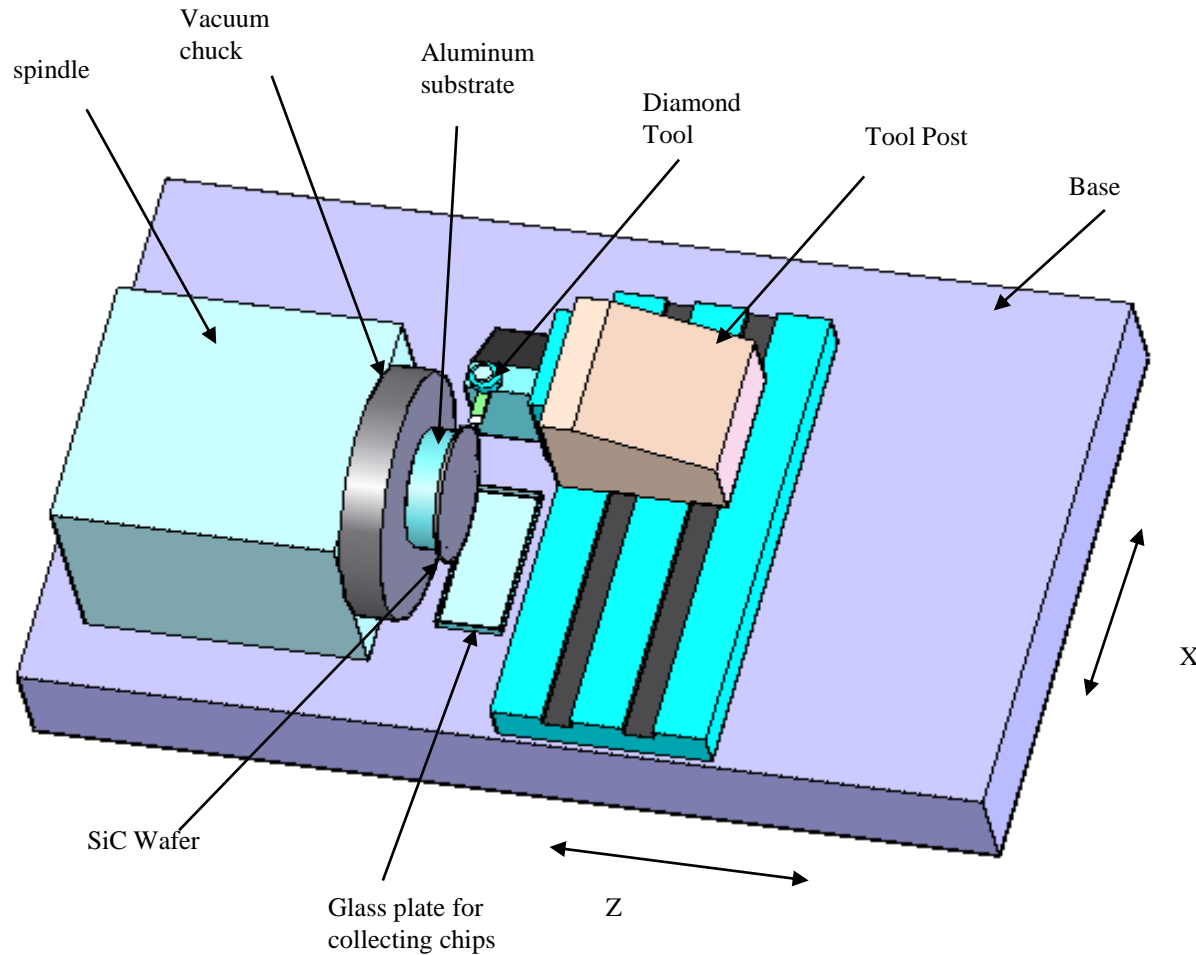
10/25/2007

AFM image of scratch I in (a) ductile (50 nm DOC), (b) transition (80 nm DOC) and (c) brittle region (500 nm DOC)

# Summary - Scratch tests on single crystal SiC

- No micro-cracks or pits were noticed in the ductile region i.e. at scratch depths less than 50 nm.
- In the transition region i.e., at depths ranging from 60-100 nm, the scratch was smooth with small deformities.
- Scratches at higher depths of cut i.e., above 150 nm were characterized by brittle cracks around the region.
- It was found that the scratch II was more brittle than scratch I in the transition region due to difference in orientation.
- Entirely ductile material removal was obtained with depths less than 60 nm .

# Edge machining tests on single crystal SiC



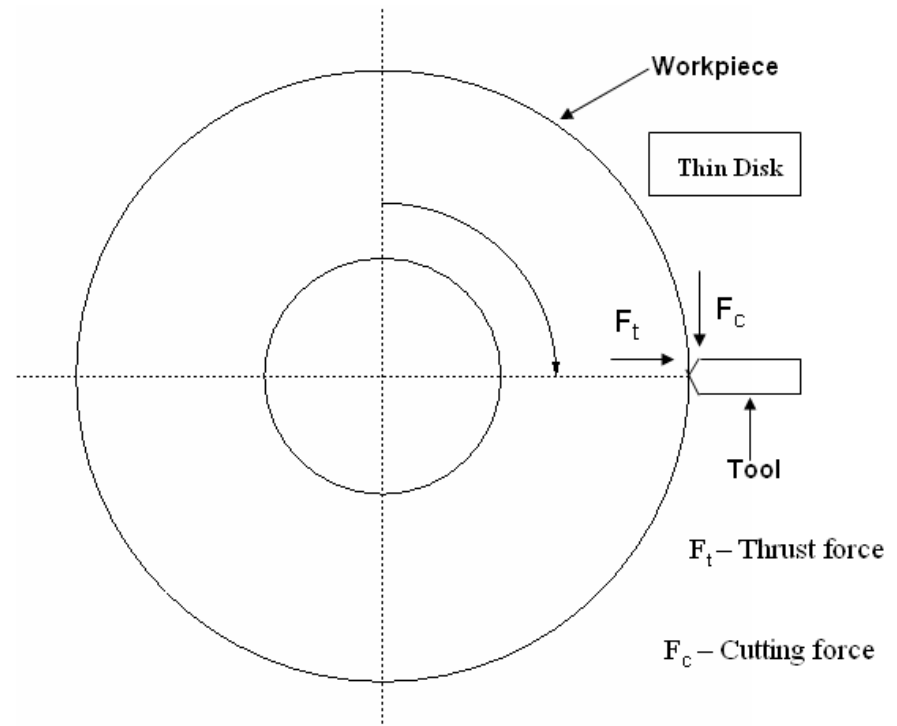
# Edge cutting - Features

Cutting is over the circumference of the workpiece.

Set up and operation is easy when compared to facing.

The process is such that orthogonal machining models are applicable.

Compared to facing, the amount of material removed is small in each pass thereby analyses of tool wear over short intervals is possible.



# Chip morphology studies

## Cutting conditions

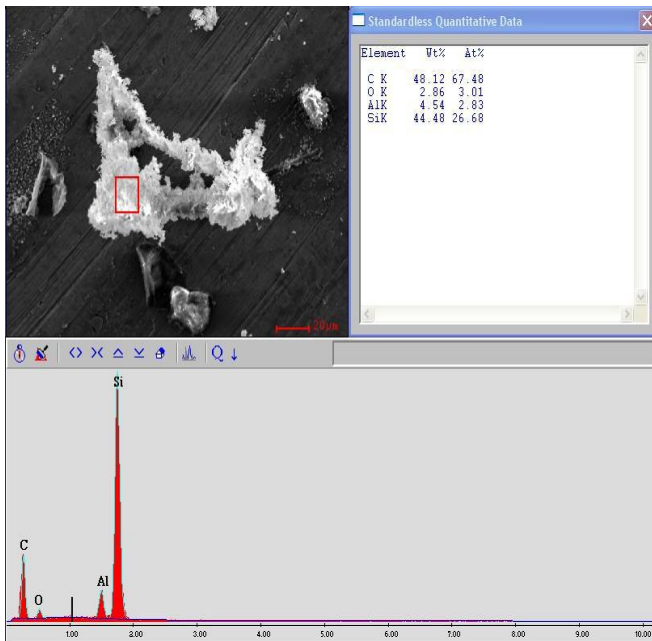
Speed of rotation (rpm) - 100

Depth of cut (nm) - 25

Feed/rev (nm/rev) - 25

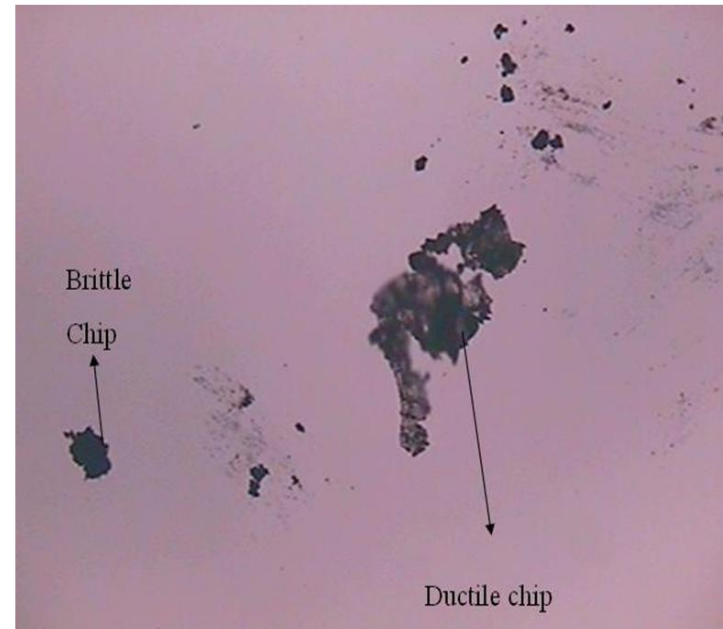
Depth of cut/min (nm/min)-2500

Total cutting time (min)- 120



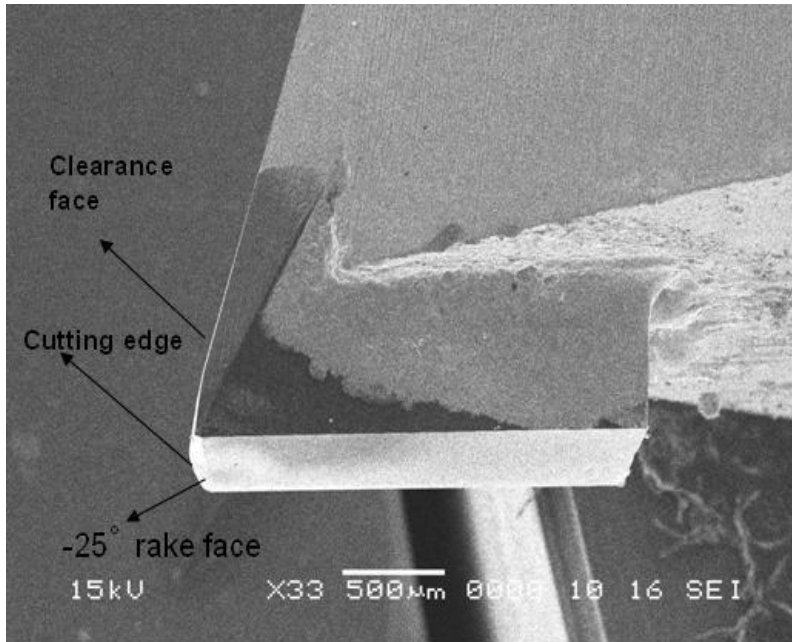
EDAX Analysis of the SiC chip

10/25/2007

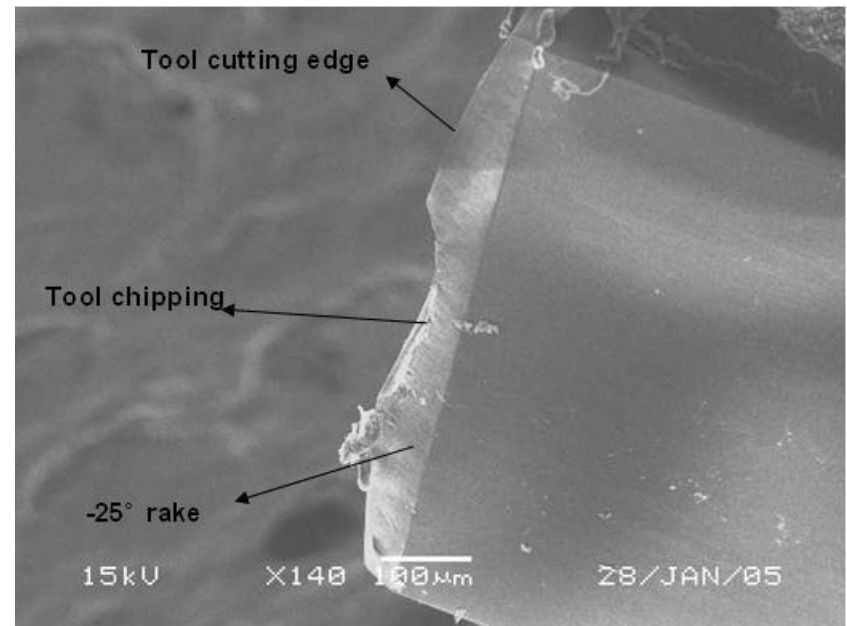


Optical microscopic image of the chip collected during the experiment.

## Tool break



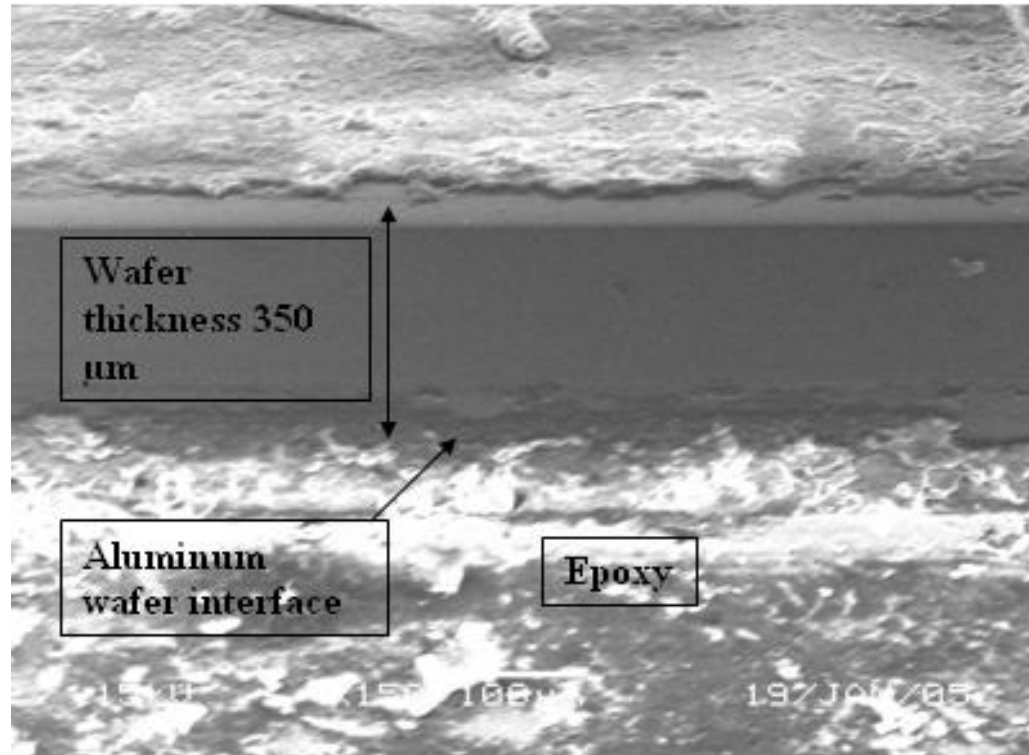
(a)



(b)

SEM image of the tool (a) before and (b) after the edge cutting experiments

# SEM images of machined wafer edges

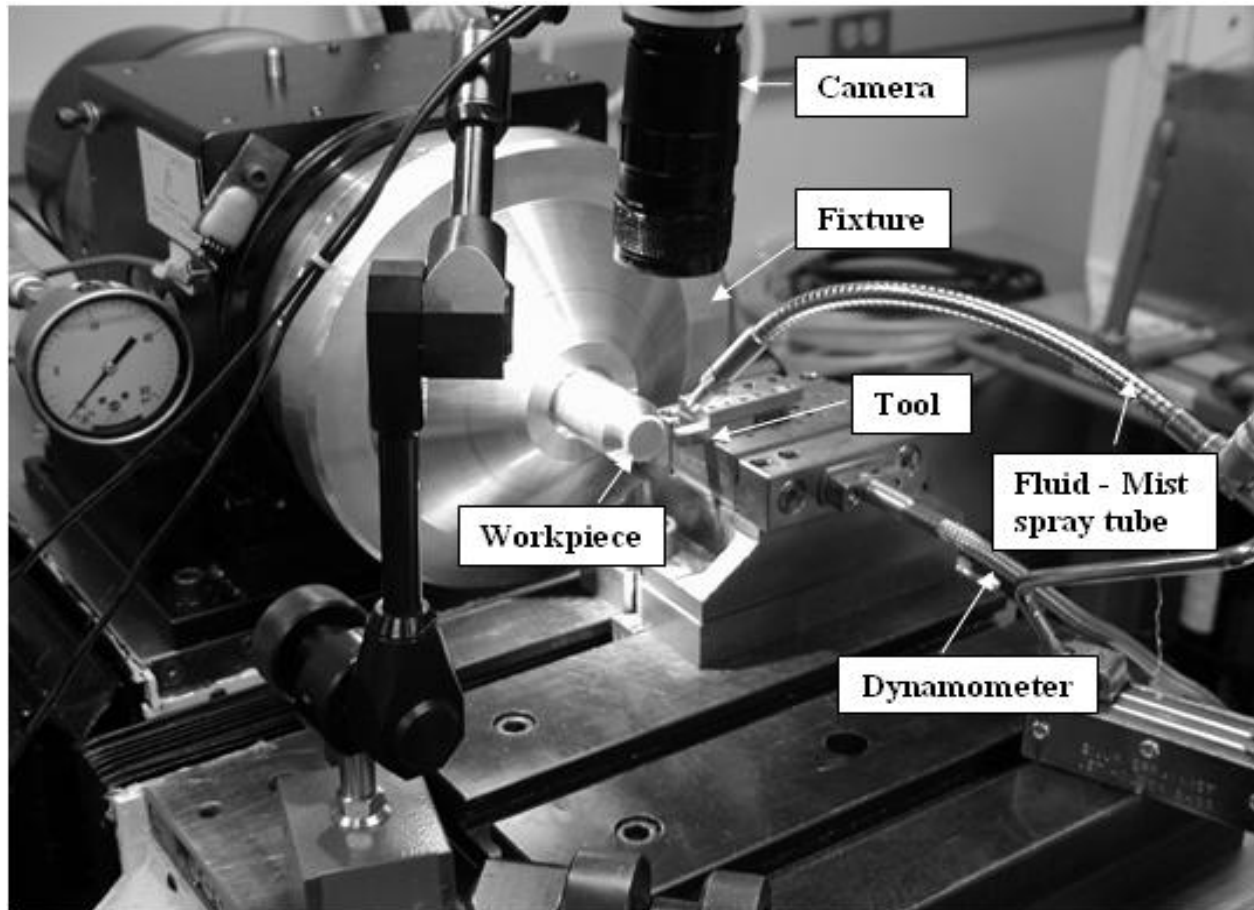


SEM image of a machined wafer edge showing a surface free of cracks or major flaws.

# Summary – Edge machining tests on single crystal SiC

- Chip morphology studies indicate the presence of long and curly chips indicating the possibility of ductile regime machining.
- Observation of machined wafer edges show a surface devoid of major cracks or flaws.
- The diamond tool stayed good for a total cutting time of approximately 120 minutes before failing catastrophically. Abrasion was believed to be the predominant tool wear mechanism causing tool wear.

# Tool wear studies during machining of silicon nitride by SPDT



Experimental Setup.

# Methodology

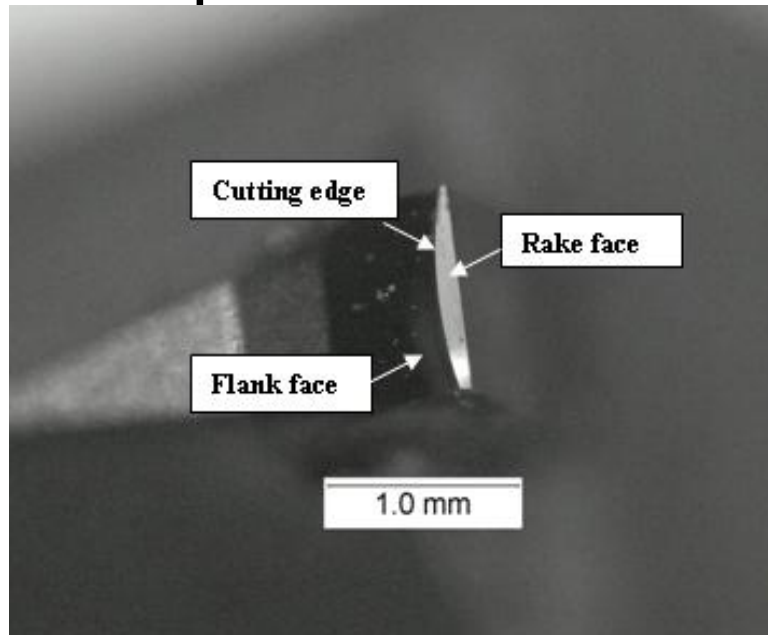
Before the start of experiments, the cutting tool was imaged using an Optical microscope.

Dynamometer was set to record the forces during machining.

Initially , truing operation was performed with a Poly Crystalline Diamond (PCD) tool. After completion, the PCD was replaced with a SCD tool and the machining experiment was started.

Each cutting experiment was started with a new unused tool. For each of the cutting experiments, when a predetermined length of cut was reached, the cutting was stopped and the cutting edge of the tool was carefully examined under an optical microscope, at a magnification factor of about 100x to check for any possible flank, rake and cutting edge wear.

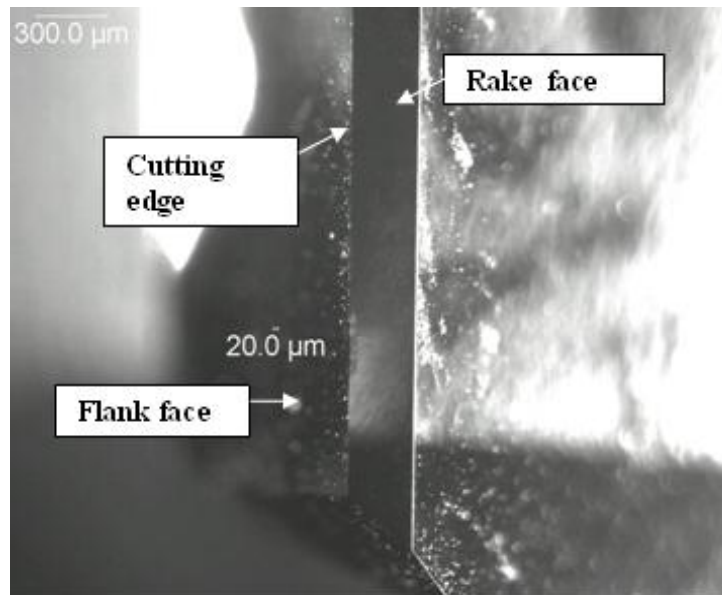
# Tool wear experiments of a radius tool



Optical microscopic image of a radius tool

Tool rake (degrees)	Depth of cut ( $\mu\text{m}$ )	Feed ( $\mu\text{m}/\text{rev}$ )	Spindle Speed (rpm)	Cutting Speed (m/s)	Cutting type	Cutting distance/pass (m)	Number of Passes
-45	0.5	0.5	100	0.105	Dry	3.142	10
-45	0.5	0.5	3000	3.15	Wet	6.284	10

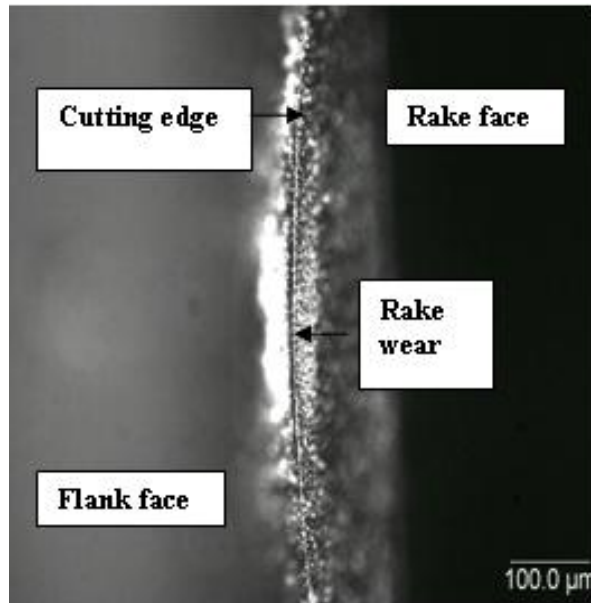
# Tool wear experiments for a straight edged tool



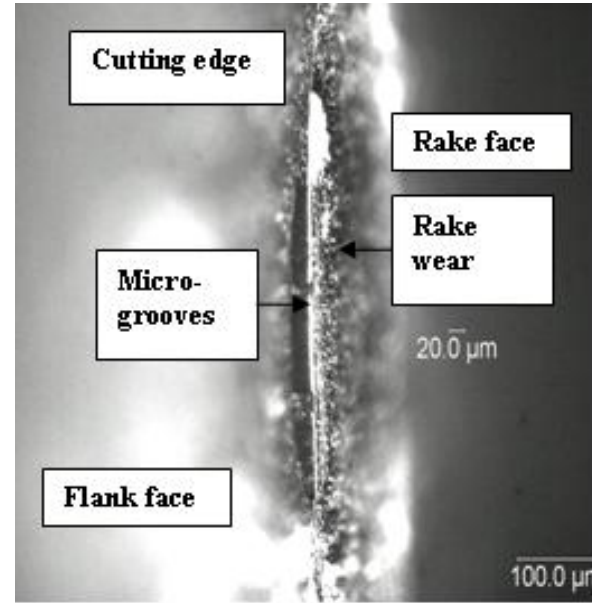
Optical microscopic image of a straight edged tool

Tool rake (degrees)	Depth of cut (μm)	Feed (μm/rev)	Spindle Speed (rpm)	Cutting Speed (m/s)	Cutting fluid	Cutting distance /pass (m)	Number of Passes
-45	0.5	0.5	3000	3.15	Dry	15.71	6
-45	0.5	0.5	3000	3.15	NIST Experimental	15.71	6
-45	0.5	0.5	3000	3.15	Mineral oil	15.71	6

## Tool wear images – Dry cutting tests with a radius tool



(a)



(b)

Optical microscope image of the nose radius tool's cutting edge for a cutting distance of (a) 3.142 m (one pass) and (b) 31.42 m (10 passes) for dry cutting tests.

## Tool wear images – Wet cutting tests with a radius tool

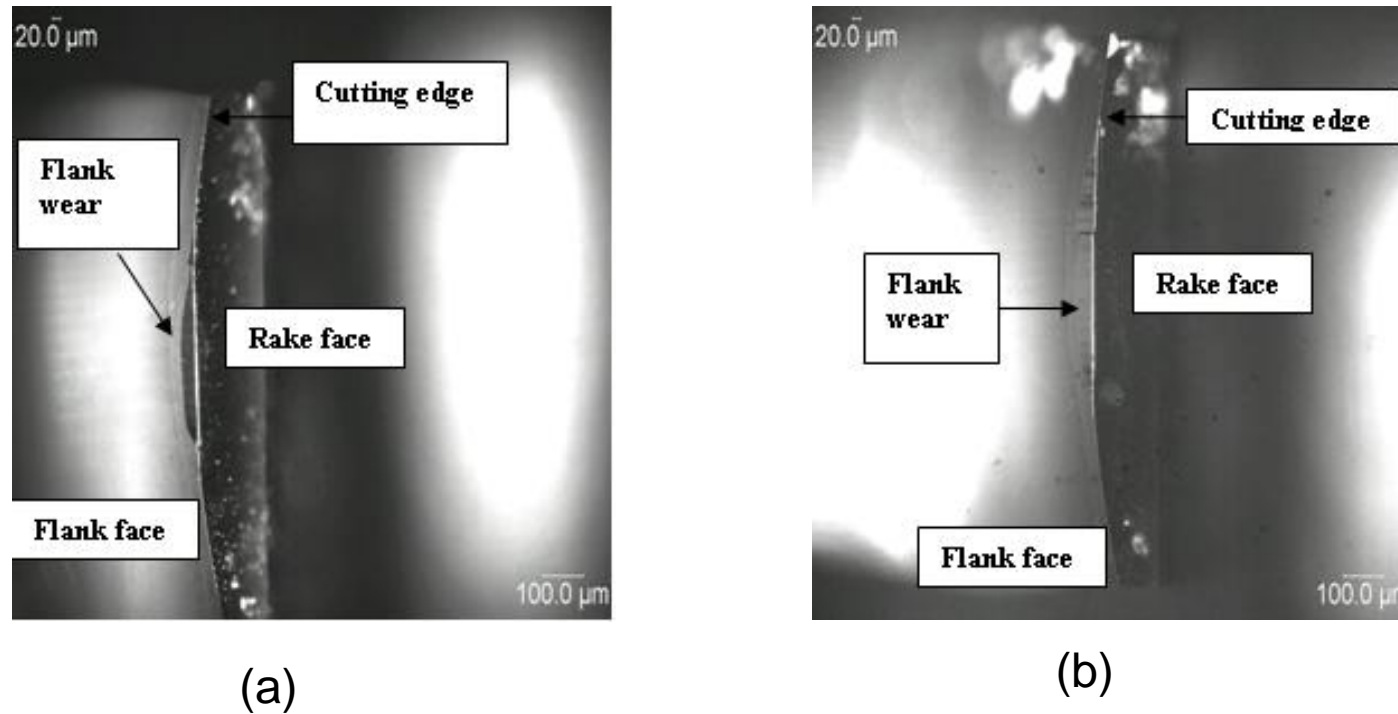
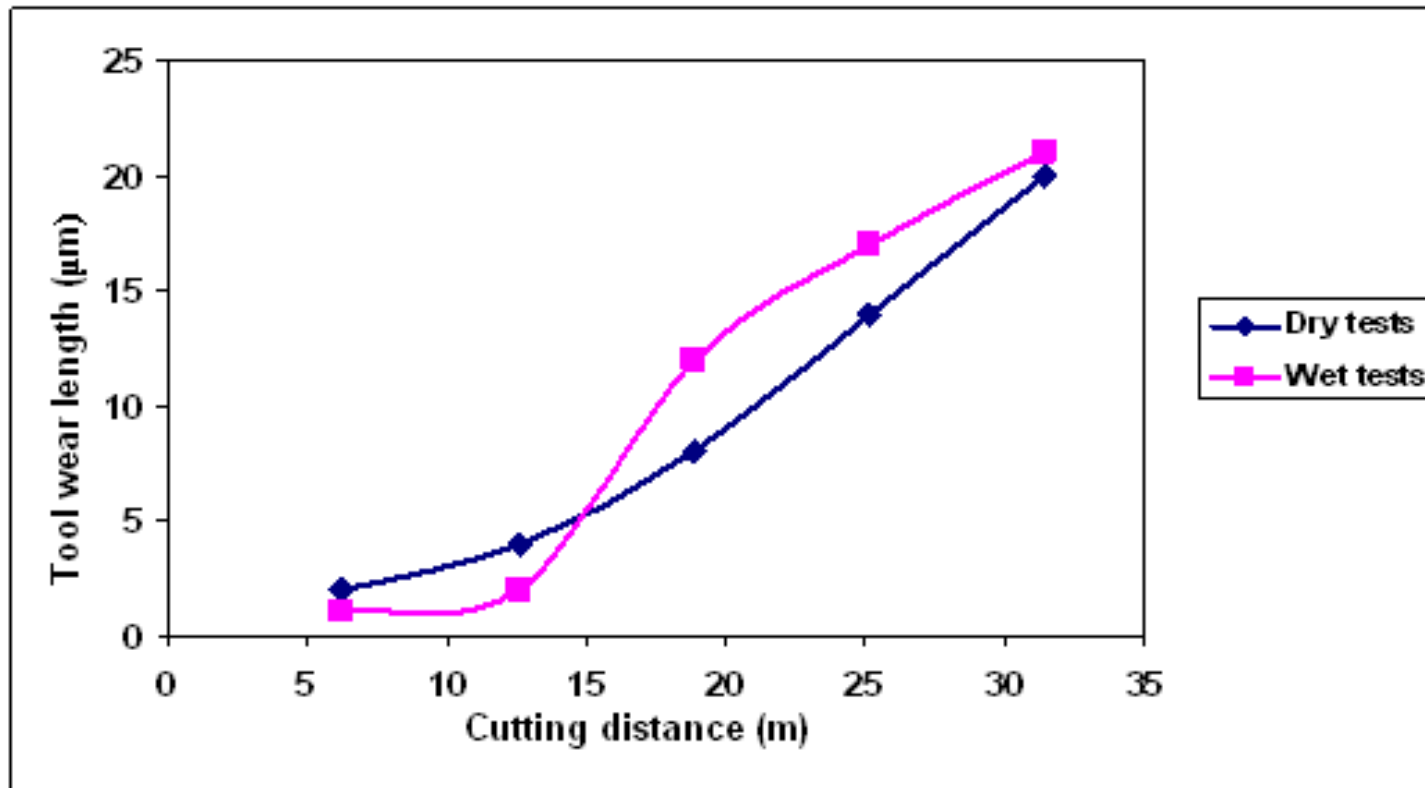


Figure 5. Optical microscope image of the tool cutting edge for a cutting distance of (a) 31.42 m (5 passes) and (b) 62.84 m (10 passes) for wet cutting tests

# Comparison of flank wear lengths – Cutting tests with a radius tool

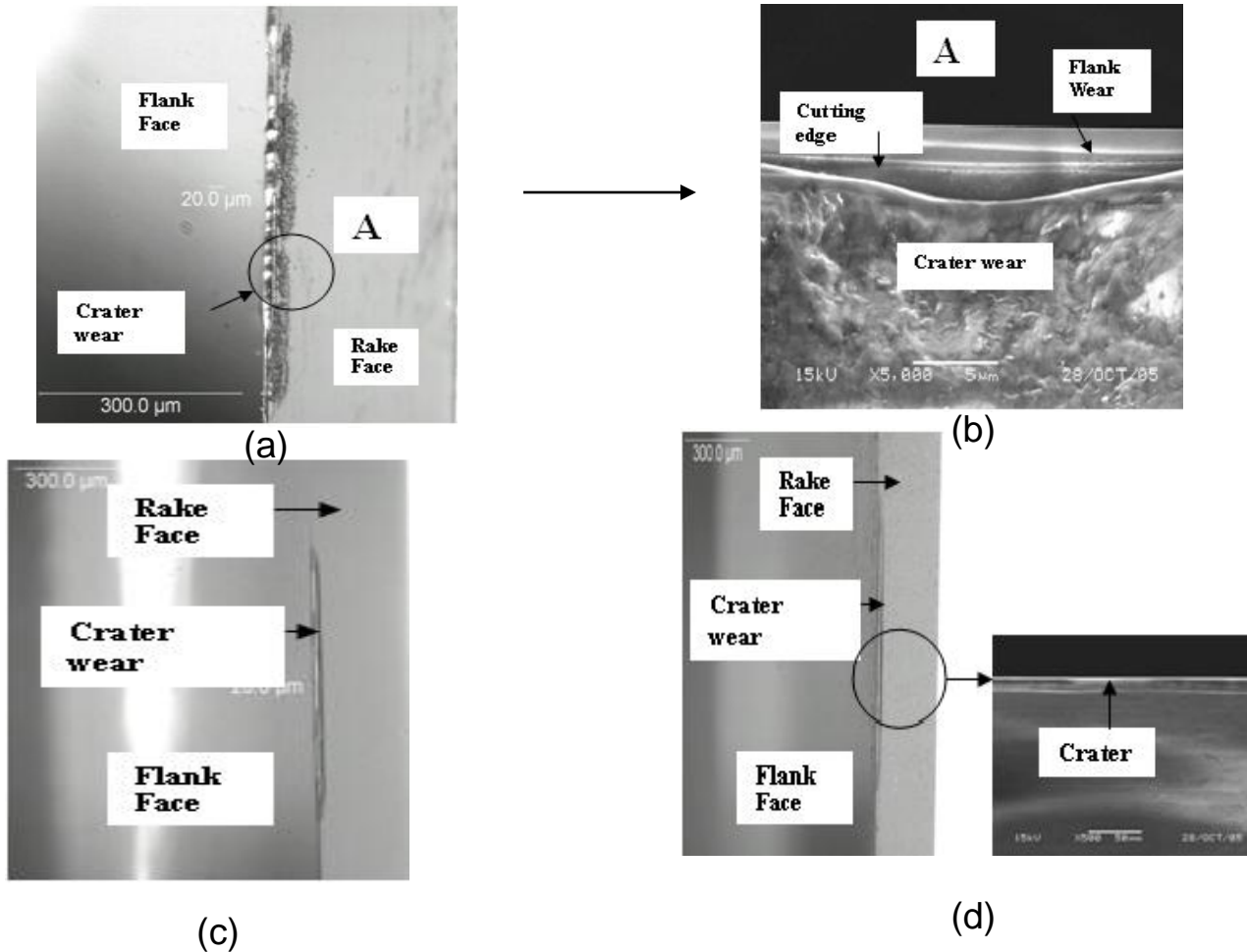


Comparisons of lengths of the tool wear land with cutting distance for dry and wet cutting tests (NIST fluid) – Cutting tests with the radius tool. Note: the wet, cutting fluid tests, were performed at a cutting speed 30 times higher than the dry cutting tests.

# Observations- Tool wear mechanisms of cutting tests with a radius tool

- For the dry tests abrasion was believed to be the dominant tool wear mechanism.
- For the wet tests a combination of abrasion and a thermally activated mechanism such as diffusion was believed to be a dominant tool wear mechanism.
- The higher Material Removal Rate (MRR) achieved at the high cutting speeds for the wet tests did not result in appreciable tool wear, and thus the NIST cutting fluid shows promise for increasing machining productivity.

# Tool wear images – Cutting tests with a straight edged tool

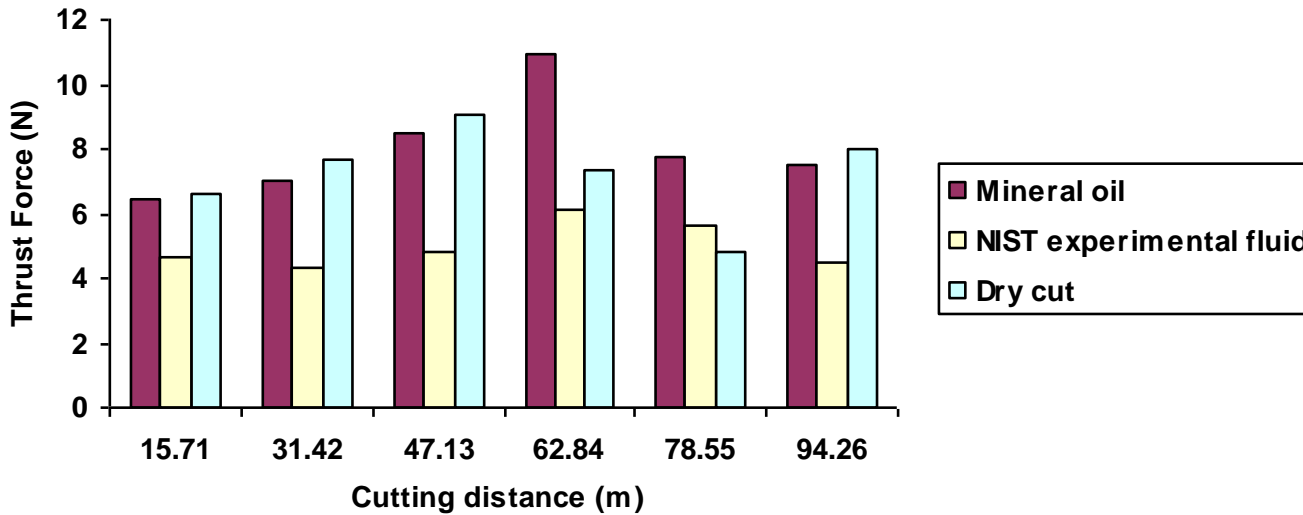


Optical microscope image of the tool cutting edge for a cutting distance of 94.26 m (6 passes) for (a) dry tests (b) SEM image of the crater wear for the dry tests (c) Mineral oil and (d) NIST experimental fluid – Cutting tests with straight edged tool

# Observations- Tool wear mechanisms of cutting tests with a straight edged tool

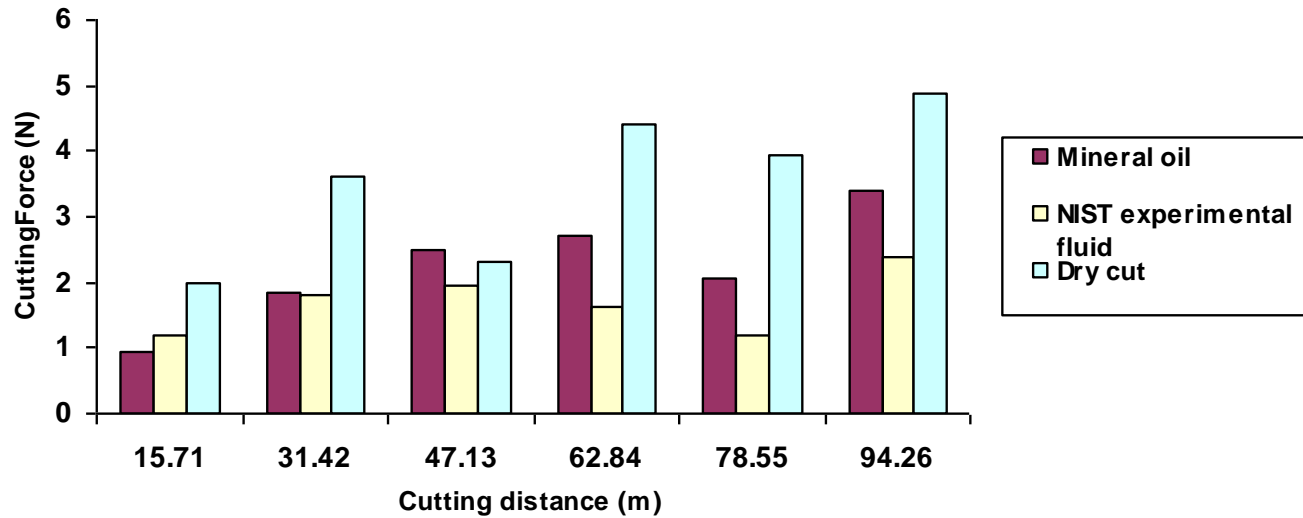
- Contrary to the wear pattern observed on a radius tool, the length of the tool wear on the rake face of the straight edge tool was greater than the length of flank wear for the given cutting distance.
- Crater wear mechanism was found to be the dominant wear mechanism.
- The extent of crater wear for dry tests were greater than the extent of crater wear in wet cutting tests.
- Reasons for difference in tool wear mechanisms between a straight edged tool and a radius tool:
  - (i) Geometry
  - (ii) Tool manufacturers – Radius tool (Edge Tech) and Straight edged tools (Chardon)

# Analysis of machining forces - cutting tests with a straight edged tool



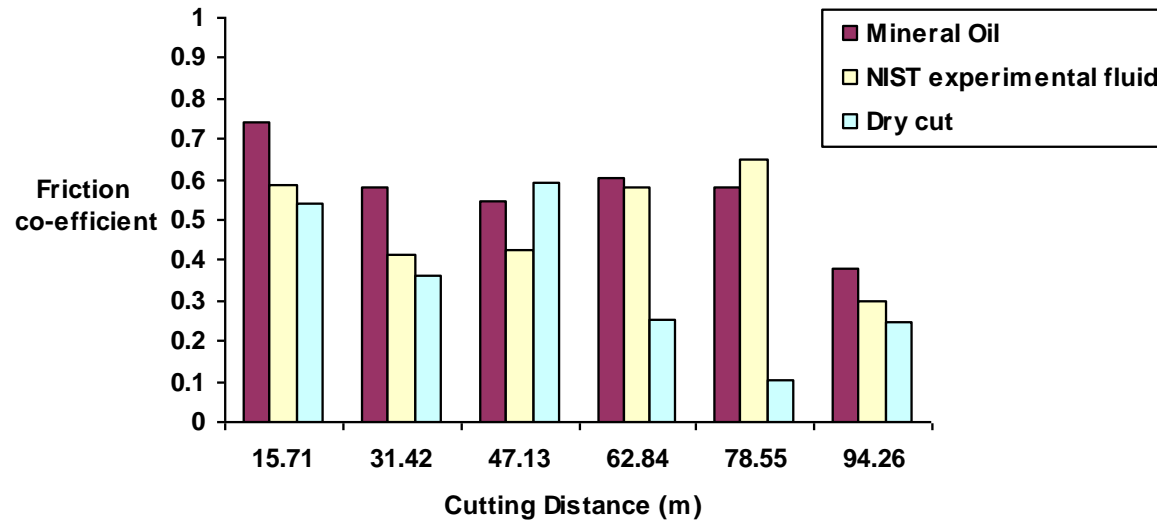
Variation of thrust forces with cutting distance

Continued ...



Variation of cutting forces with cutting distance

Continued ...

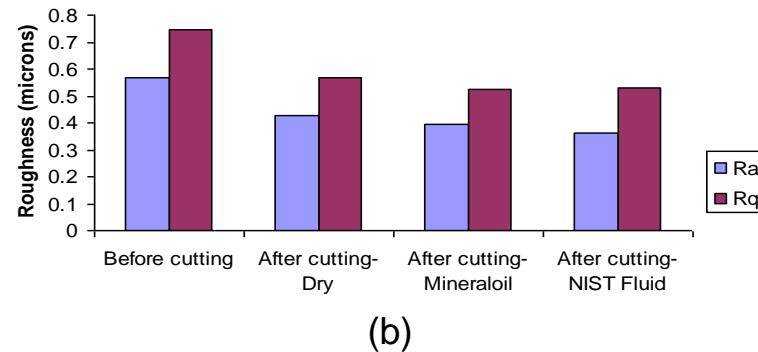
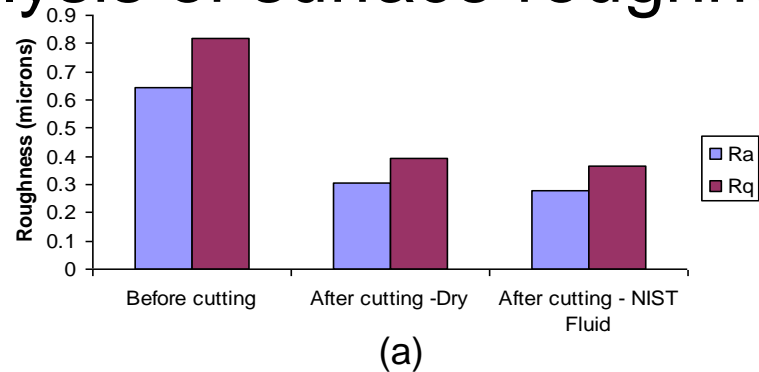


Variation of “apparent” friction co-efficient ( $\mu_a$ ) with cutting distance -for cutting tests with a straight edged tool

# Results – Force analysis

- Comparison of cutting and thrust forces show that the thrust force dominated the cutting force throughout the period of cutting as observed with the radius tool.
- NIST fluid was most often the best in terms of lowering the thrust and cutting forces, which confirms the assumption that the NIST cutting fluid performs better under high temperature cutting conditions.
- Since crater wear is always accompanied by flank wear, the cutting force component was found to be greater for the dry tests. This was due to the frictional force component measured as part of cutting force.
- For both the dry and the wet cutting tests, the coefficient of friction decreased with the cutting distance.

# Analysis of surface roughness



Variation of surface roughness with cutting distance for cutting tests with (a) radius tool and (b) straight edged tool

## Observations:

Analyses of machined workpiece edges had shown that the machining tests with the radius (Edge Tech) tool produced a better surface finish than the machining tests with the straight edged (Chardon) tool.

NIST fluid was found to provide a beneficial effect by lowering the forces and better surface finish.

# Overview of Numerical studies

- Drucker-Prager Constitutive model
- Nano-indentation simulations of SiC with a diamond indenter using Abaqus/Standard.
- Orthogonal machining simulations of SiC with a single point diamond tool using Abaqus/Explicit.

# Drucker – Prager material model

$$f = \sqrt{3J_2} + \frac{1}{3}I_1\alpha - k = 0$$

$f$  - Yield function.

$J_2$  - Second invariant of the deviatoric stress tensor,  $S_{ij}$

$I_1$  - First invariant of the stress tensor

$\alpha$  - Pressure sensitivity co-efficient

$k$  - Cohesion of the material.

$$\alpha = \frac{1}{3\sqrt{3}} \tan(\beta)$$

$\beta$  - Angle of internal friction of the material

# Non-Associative flow rule – plastic potential

$$\pi = \sqrt{3J_2} + \frac{1}{3}I_1\delta = 0$$

where the material parameter ' $\delta$ ' is called the dilatancy factor

For associative flow rule ' $\beta=\delta$ '

For non-Associative flow rule ' $\beta\neq\delta$ '

Phase transformations in SiC are accompanied by a volume reduction

In ABAQUS, the value of friction angle  $\beta < 0$  is not premissible

For volume reduction,  $\delta < 0$  always hence ' $\beta \neq \delta$ '

To describe phase transformation problems accompanied by volume reduction only non-associative flow rule could be used

# Drucker- Prager parameters in ABAQUS

In Abaqus the Drucker-Prager model is defined by the parameters:

$\psi$  -Dilation angle,  $\beta$  -Friction angle and

$K$  -The ratio of yield strength in tri axial tension to compression

$$\delta = \tan(\psi).$$

$$\tan \beta = \frac{6 \sin \phi}{3 - \sin \phi}$$

$$K = \frac{3 - \sin \phi}{3 + \sin \phi}$$

Continued.....

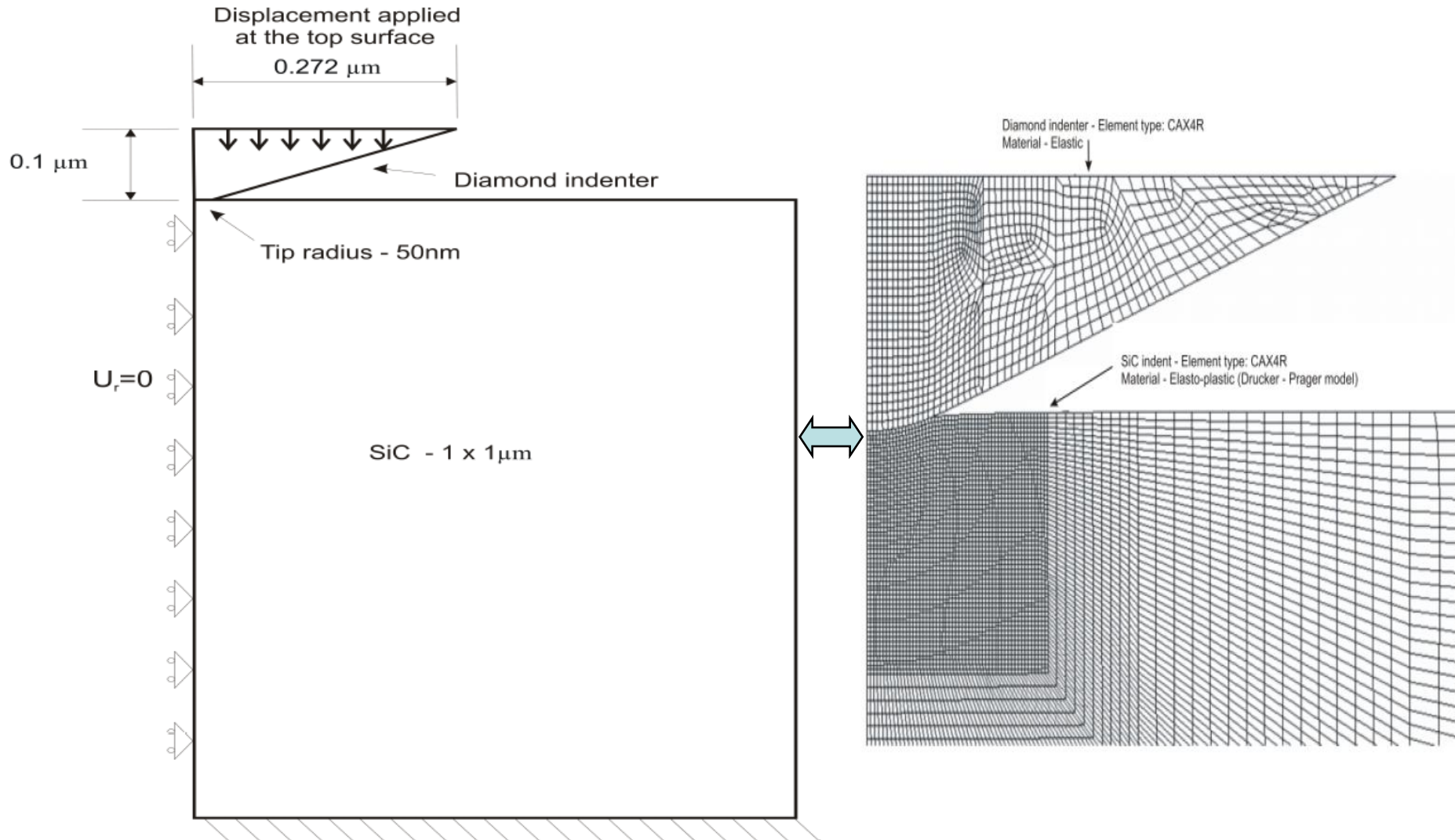
Here  $\phi$  is the Mohr-Coulomb friction angle and is obtained by

$$\phi = \sin^{-1} \left( \frac{\sigma_c - \sigma_t}{\sigma_c + \sigma_t} \right)$$

Here  $\sigma_c$  and  $\sigma_t$  are uniaxial compressive and tensile stresses

Note: The Drucker-Prager parameters are obtained from the Mohr-Coulomb friction angle by parameter matching

# Nano-indentation of SiC – FE model

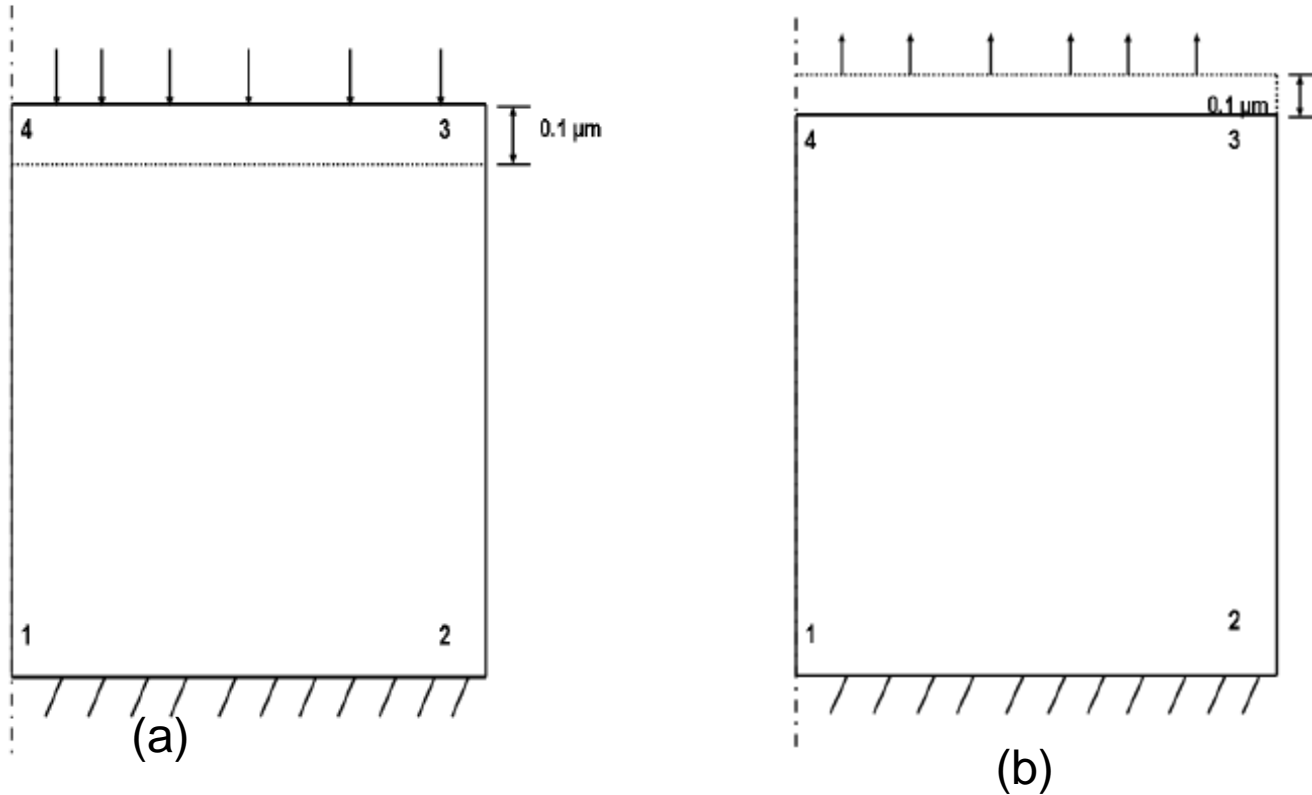


Drucker-Prager parameters for various values of strength ratio  $\left(\frac{\sigma_t}{\sigma_c}\right)$

$\left(\frac{\sigma_t}{\sigma_c}\right)$	$(\beta)$	$K$
0.1	66	0.571
0.2	59.74	0.63
0.3	52.69	0.695
0.4	45	0.75
0.5	36.86	0.8
0.6	28.61	0.846
0.7	20.55	0.88
0.8	12.99	0.92
0.9	6.11	0.965
1	0	1

In ABAQUS, to maintain the convexity of the yield surface, the condition  $K \geq 0.778$  should be satisfied

# One element test



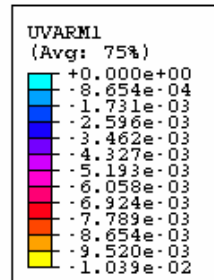
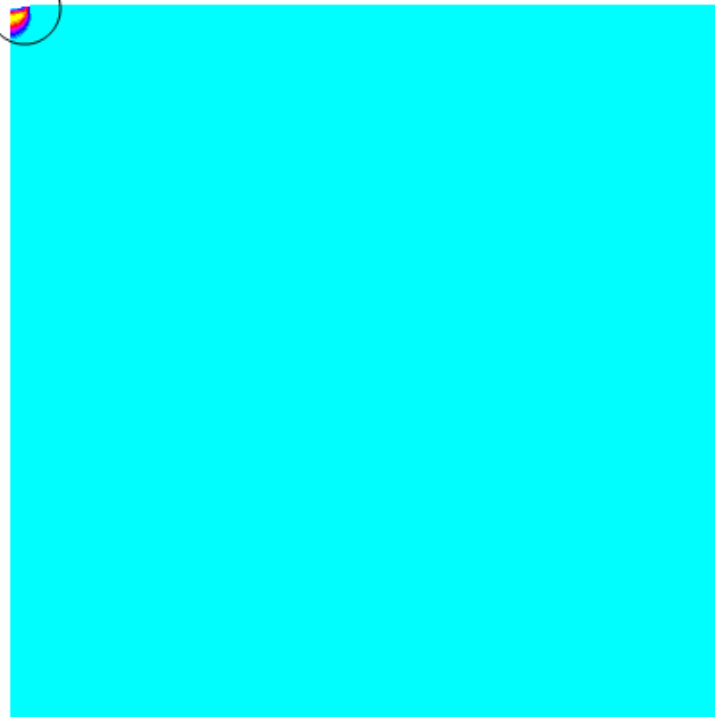
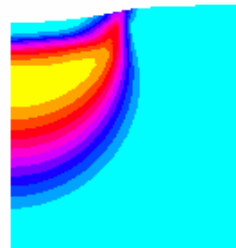
One element test in (a) compression and (b) tension;  
 Element type : CAX4R; Dimensions :  $1 \times 1 \mu\text{m}$ .

Strength ratio ( $\frac{\sigma_t}{\sigma_c}$ ) obtained for varying Drucker-Prager parameters - One element test.

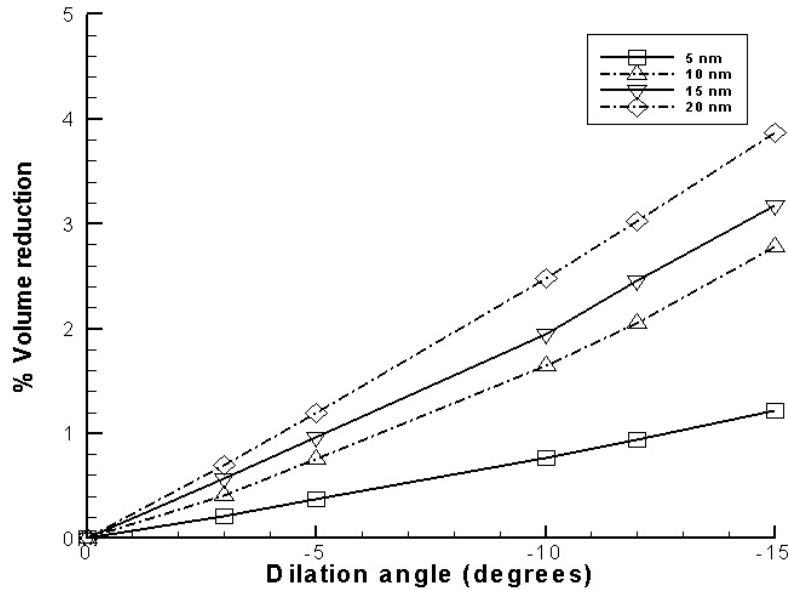
$(\frac{\sigma_t}{\sigma_c})_{analytical}$	$(\beta)$	$K$	$(\frac{\sigma_t}{\sigma_c})_{simulation}$	% difference
0.1	66	0.778	0.134	34
0.2	59.74	0.778	0.221	10.5
0.3	52.69	0.778	0.317	5.66
0.4	45	0.778	0.411	2.75
0.5	36.86	0.8	0.504	0.8
0.6	28.61	0.846	0.601	0.16
0.7	20.55	0.88	0.701	0.14
0.8	12.99	0.92	0.801	0.125
0.9	6.11	0.965	0.901	0.11
1	0	1	1	0

# Contour plot – volume change after loading

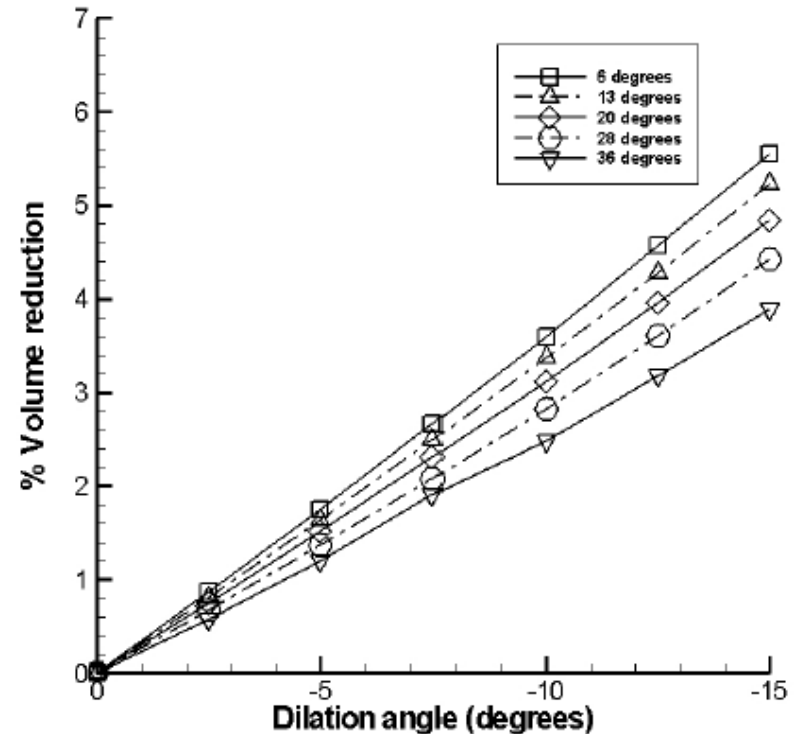
Maximum  
volume change  
1.039 %



# Volume change with respect to different material parameters

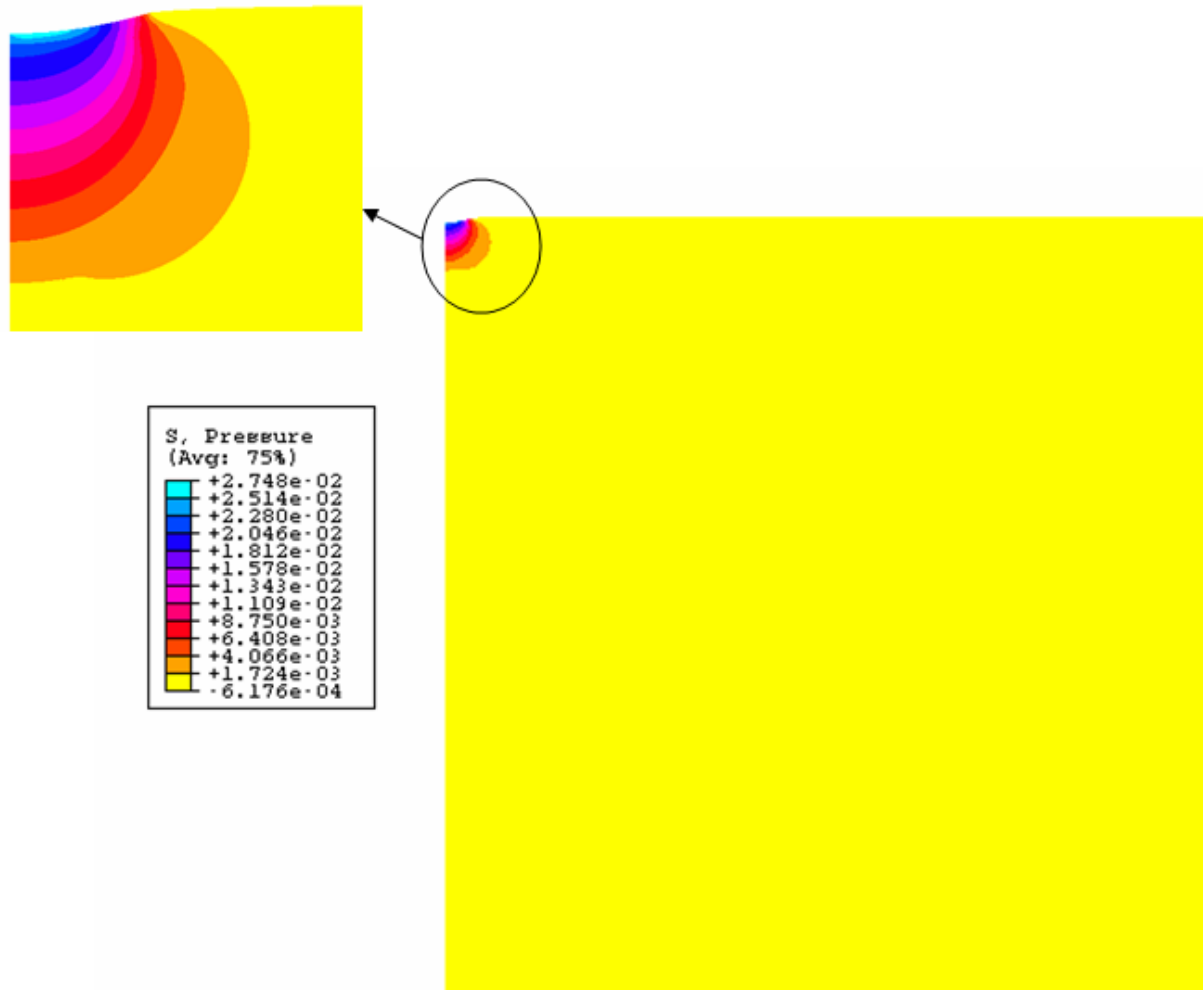


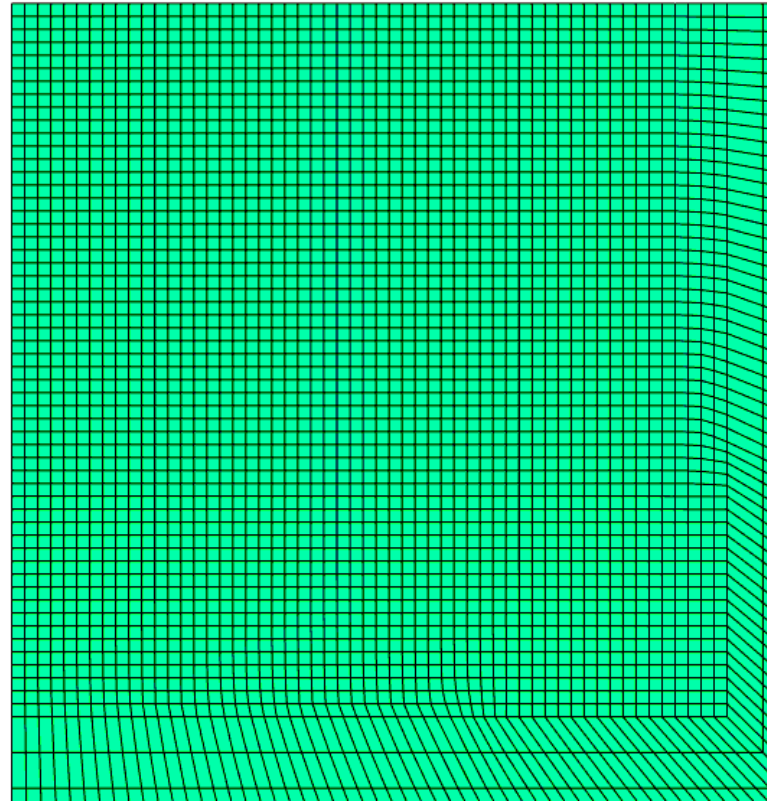
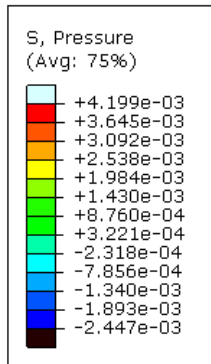
% Volume reduction vs dilation angle for various depths of indentation after unloading.



% Volume reduction vs dilation angle for various friction angles after unloading.

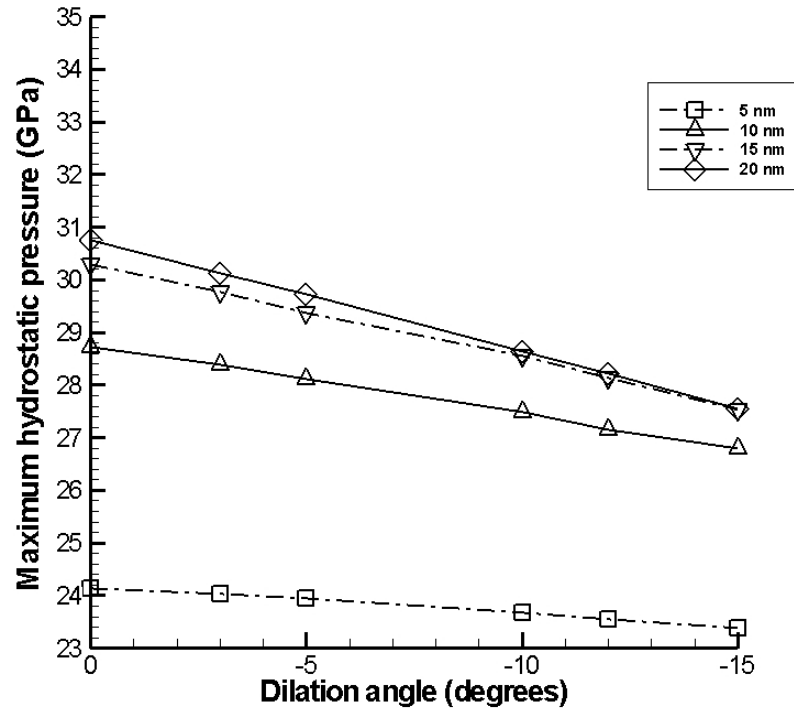
# Plot of hydrostatic pressures ( $\times 10^{12}$ Pa) after loading



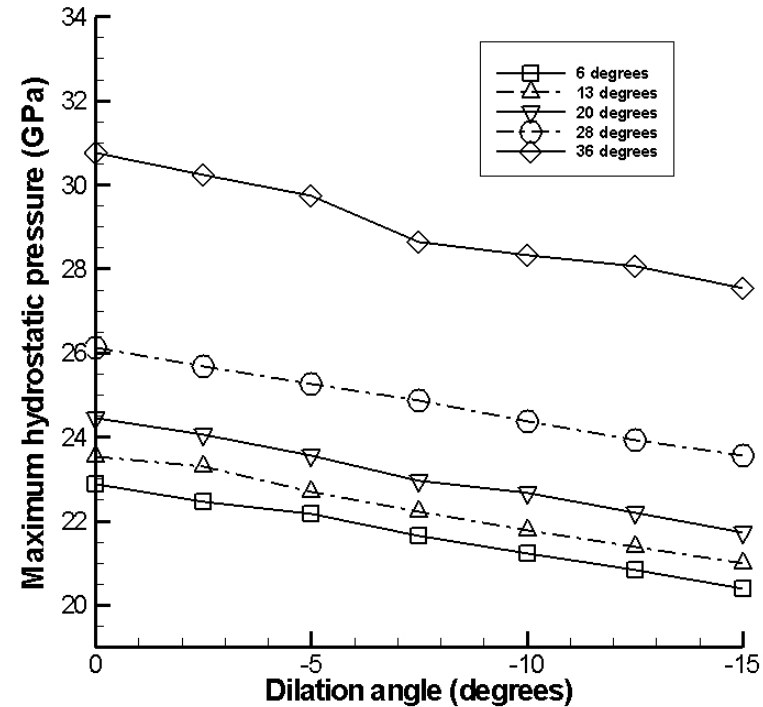


Nano-indentation simulation : Time-history plot of hydrostatic pressure

# Maximum hydrostatic pressure with respect to different material parameters



Maximum hydrostatic pressure vs dilation angle for various depths of indentation after loading.



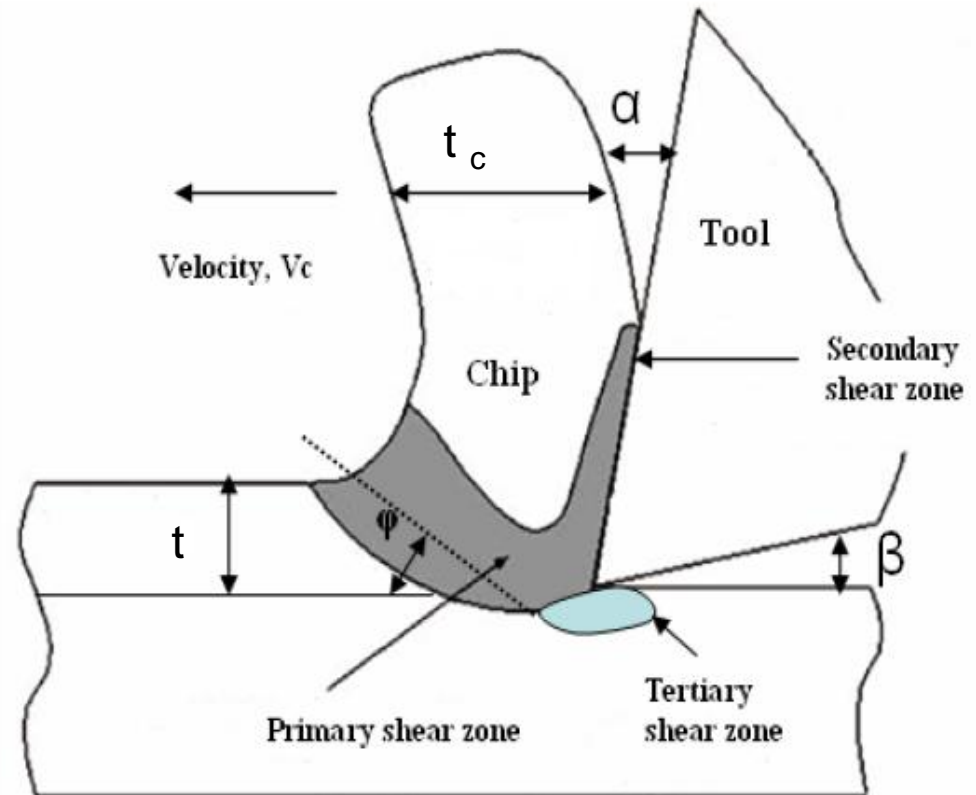
Maximum hydrostatic pressure vs dilation angle for different friction angles after loading.

# Summary

- An attempt was made to describe the volume changes associated with phase transformations by considering a non-associative flow rule with negative dilation angles.
- The numerical studies indicate that the percent volume reduction increases as the dilation angle decreases.
- The volume changes predicted are at most 5%, which is significantly lower than the 20% (or higher) reduction reported in the literature.
- The predicted values of the hydrostatic pressure are in excess of the hardness value of SiC at the onset of yield, thus indicating that the present model is capable of capturing the possible ductile behavior of SiC.

# Orthogonal machining simulations

- The cutting edge of the tool is perpendicular to the direction of tool motion.
- The chip does not flow either side of the workpiece.
- The depth of cut is constant.
- The tool moves relative to the workpiece with a uniform velocity.
- The chip flow direction is normal to the cutting edge.



Schematic of a Orthogonal cutting operation:  $t_c$  - Chip thickness,  $t$  – uncut chip thickness (depth of cut)

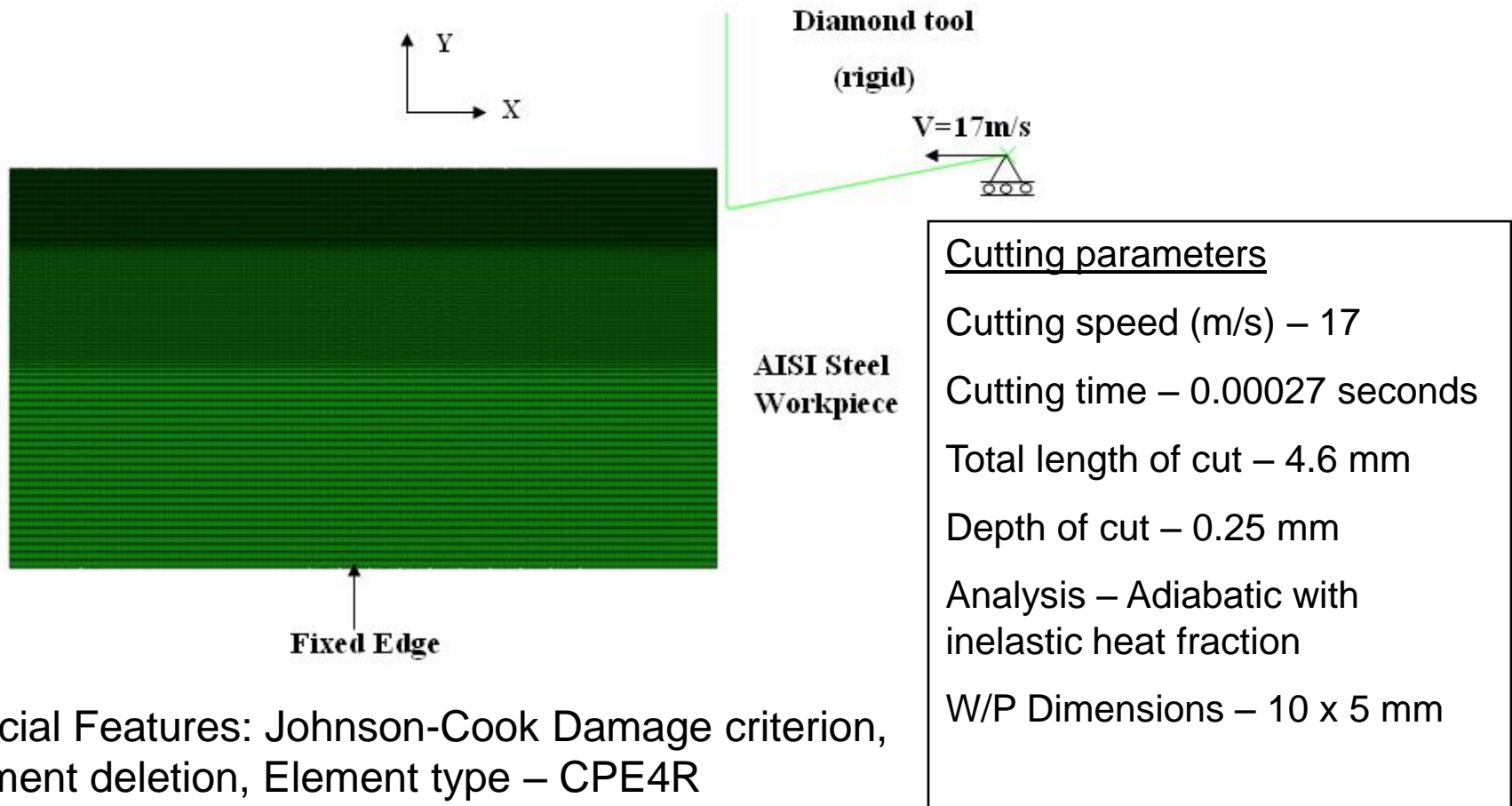
## Orthogonal machining simulation of metals - Johnson-Cook model

$$\bar{\sigma} = [A + B(\bar{\epsilon}^p)^n] \left[ 1 + C \ln \left( \frac{\dot{\bar{\epsilon}}^p}{\dot{\epsilon}_0} \right)^m \right] \times \left[ 1 - \left( \frac{T - T_0}{T_m - T_0} \right) \right]$$

where  $A$  is the yield stress,  $B$  is the strength coefficient,  $C$  is the strain rate constant,  $T$  is the temperature,  $\bar{\sigma}$  is the stress,  $T_m$  is the melting temperature,  $T_0$  is the reference temperature,  $n$  is the strain-hardening exponent and  $m$  is the thermal softening exponent.

In the Johnson Cook model, the flow stress is dependent on strain, strain rate and temperature.

# Johnson-cook model with material separation



# Material properties of AISI 4340 steel

$A(\text{MPa})$	792
$B(\text{MPa})$	510
$C$	0.014
$m$	1.03
$n$	0.26
Reference strain rate, $\dot{\epsilon}_0$	1
$D_1$	0.05
$D_2$	3.44
$D_3$	-2.12
$D_4$	0.002
$D_5$	0.61
$T_m$ °C	1520
Density $kgm^{-3}$	7830
Poisson's ratio	0.3
Specific heat $JKg^{-1}K^{-1}$	477
Thermal Expansion co-efficient	$11.5 \times 10^{-6}$
Inelastic heat fraction	0.9

Johnson-Cook damage criterion

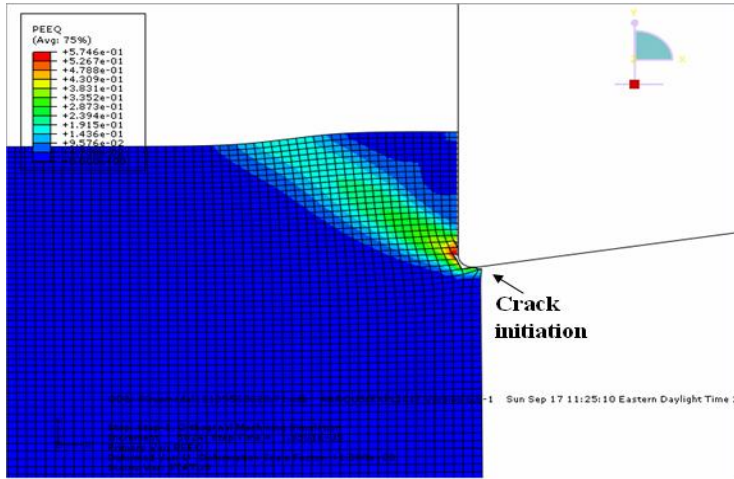
$$\bar{\epsilon}^{p^f} = (D_1 + D_2 \exp D_3 \sigma^*) \left( 1 + D_4 \ln \frac{\dot{\epsilon}^p}{\dot{\epsilon}_0} \right) \left[ 1 - D_5 \left( \frac{T - T_0}{T_m - T_0} \right) \right]$$

$$D = \sum \frac{\Delta \bar{\epsilon}^p}{\bar{\epsilon}^{p^f}}$$

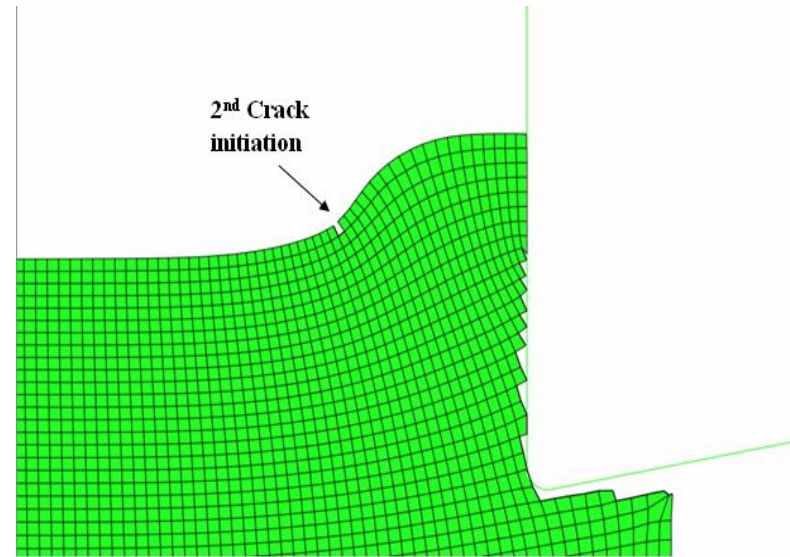
$D_1$  to  $D_5$  - Failure parameters

Courtesy: Y.B. Guo

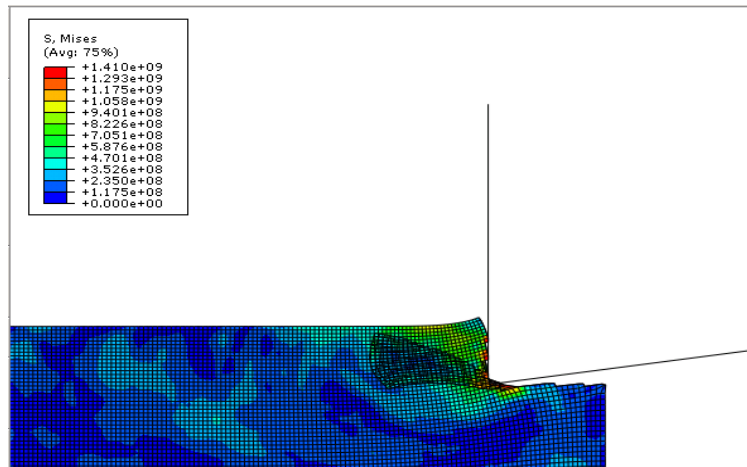
# Mechanism of Chip formation



(a)

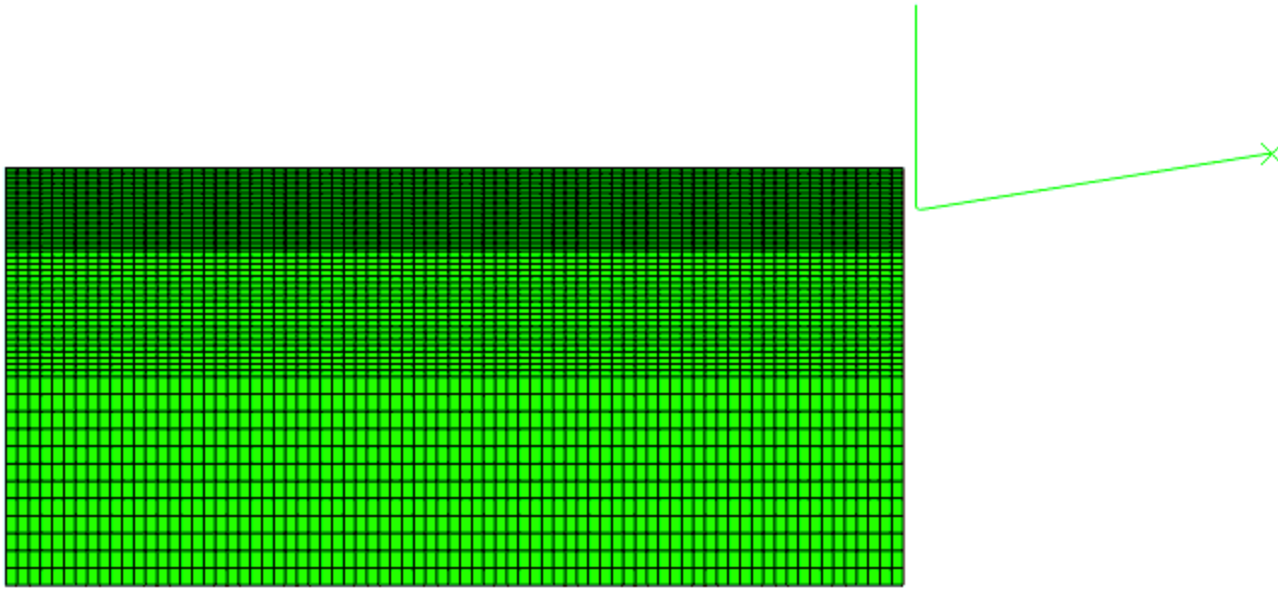


(b)



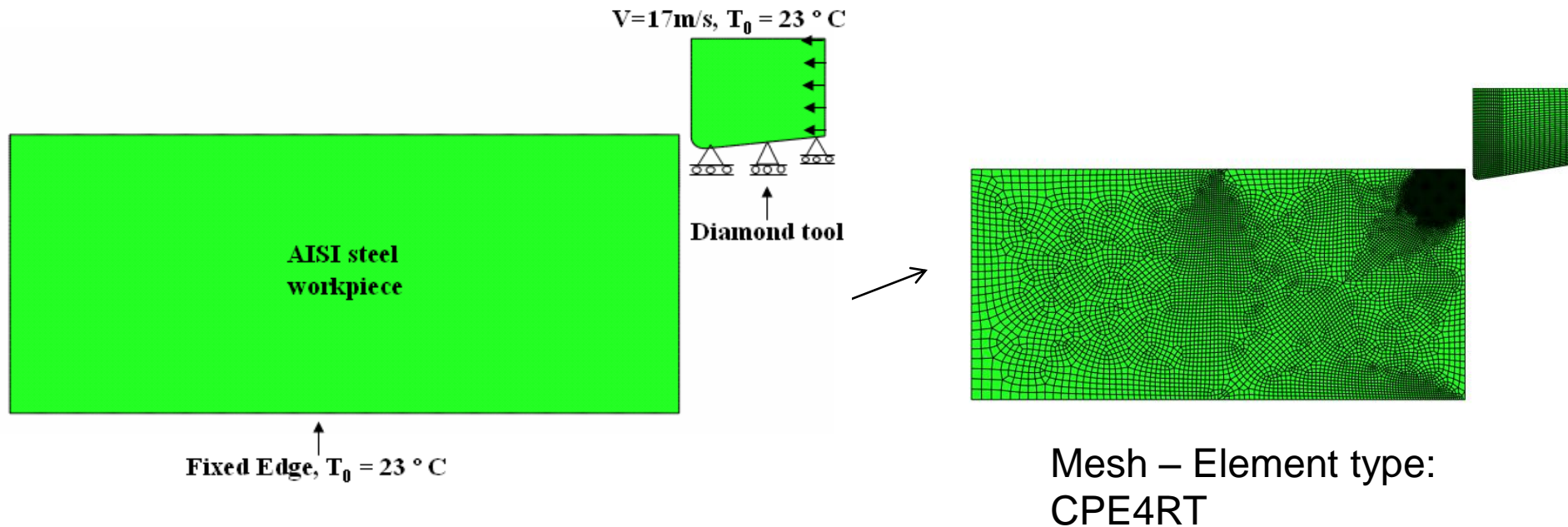
(c)

Deformed shape of the workpiece after (a) crack initiation at the tool-workpiece interface, (b) 2<sup>nd</sup> crack initiation at the free edge and (c) chip formation after the combination of the two crack fronts



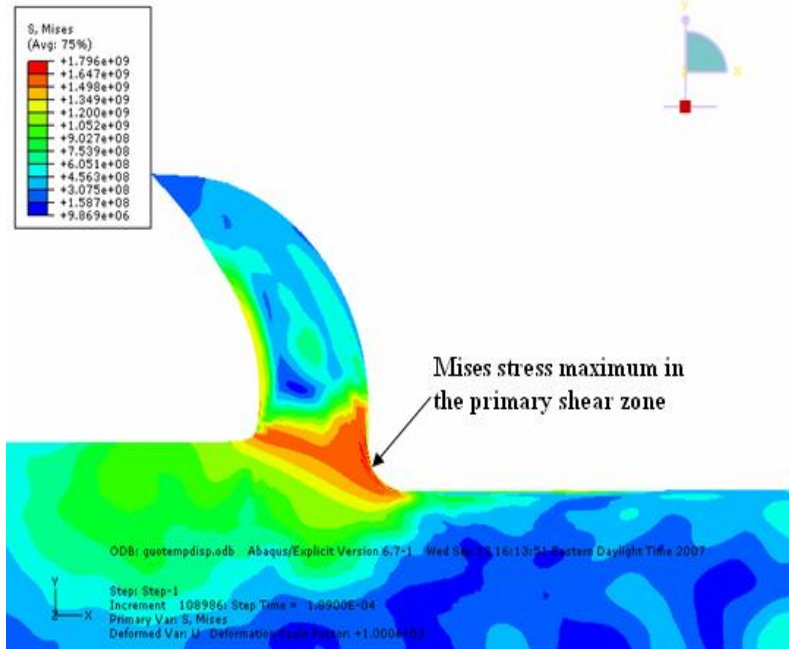
Deformed shape of the tool after 4.6 mm cutting length -Curly chip formation.

# Machining model of steel with no material separation

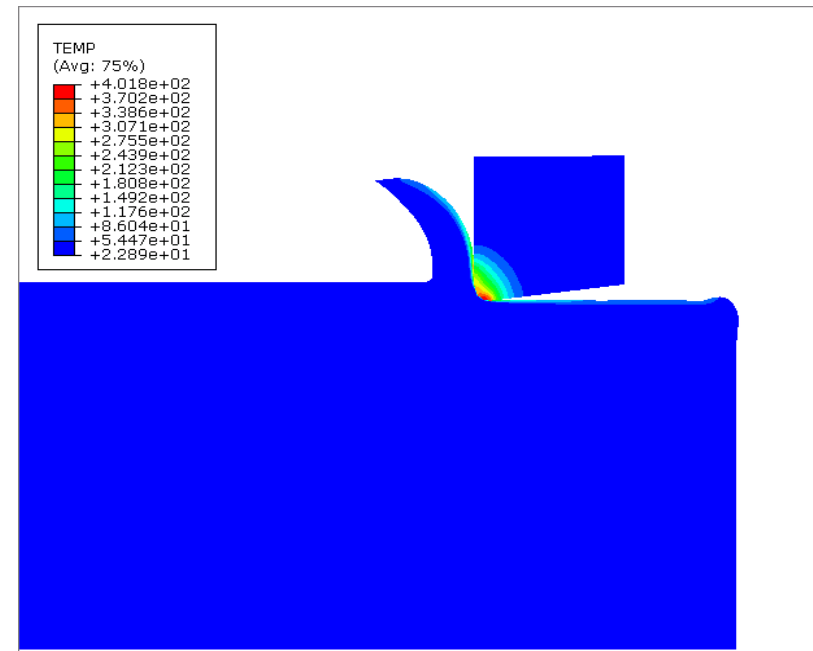


Special Features: Coupled temp-Displacement analysis,  
 Diamond tool is elastic and deformable, Initial  
 temperature  $T_{\text{initial}} = 23^\circ\text{C}$ , Element Type – CPE4RT,  
 ALE Formulation

# Temperature and stress plots at the end of cutting



(a)



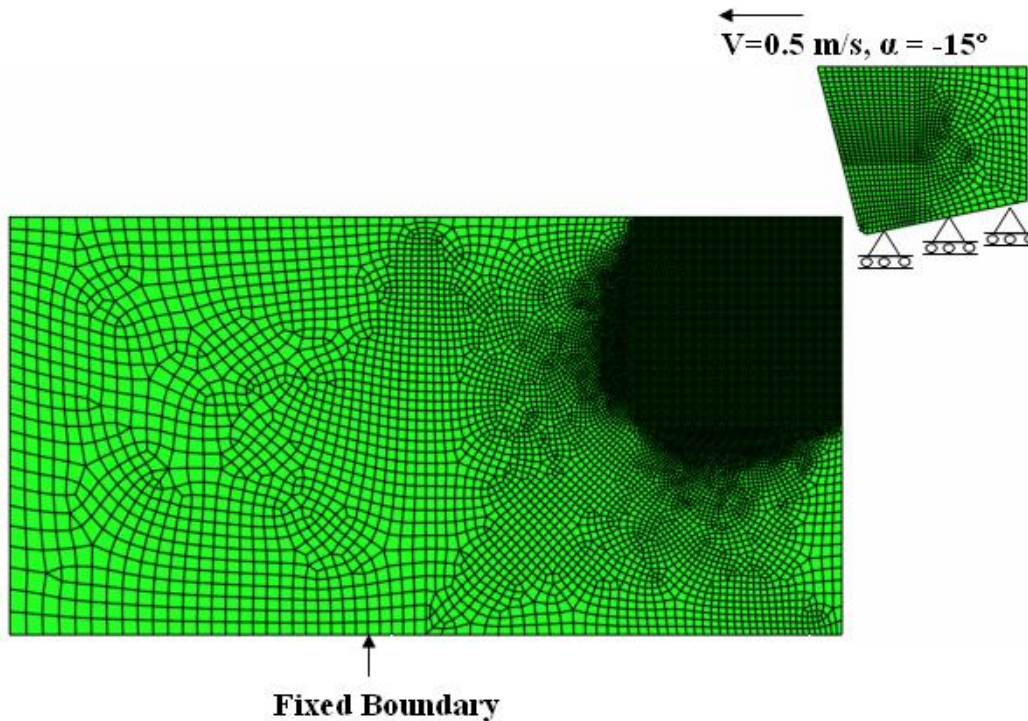
(b)

Contour plot showing (a) Mises stress (Pa) and (b) Temperature ( $^{\circ}$  C) in the model

# Summary – machining simulations of steel

- Both the Mises stress and temperature results were found to agree with previous published works from the literature.
- The simulation results give us a starting point for modeling ductile regime machining of a pressure dependent material such as SiC.

# Orthogonal machining simulation of SiC using Drucker-Prager material model



## Cutting parameters

Cutting speed (m/s) – 0.5

Cutting time – 5  $\mu$ s

Depth of cut – 100 nm

W/P Dimensions – 5 x 2.5  $\mu$ m

Mass scaling –  $10^4$  (uniform)

Special Features: Pressure dependent material model, non-associative, considers volume reduction, Element Type – CPE4R, ALE Formulation, workpiece and geometry modeled in 0.1 mm base units

# Material Properties

Elastic modulus, $Nm^{-2}$	$1000 \times 10^9$
Density, $kgm^{-3}$	3350
Poisson's ratio	0.07
Specific heat, $JKg^{-1}K^{-1}$	520
Thermal conductivity, $Wm^{-1}K^{-1}$	700

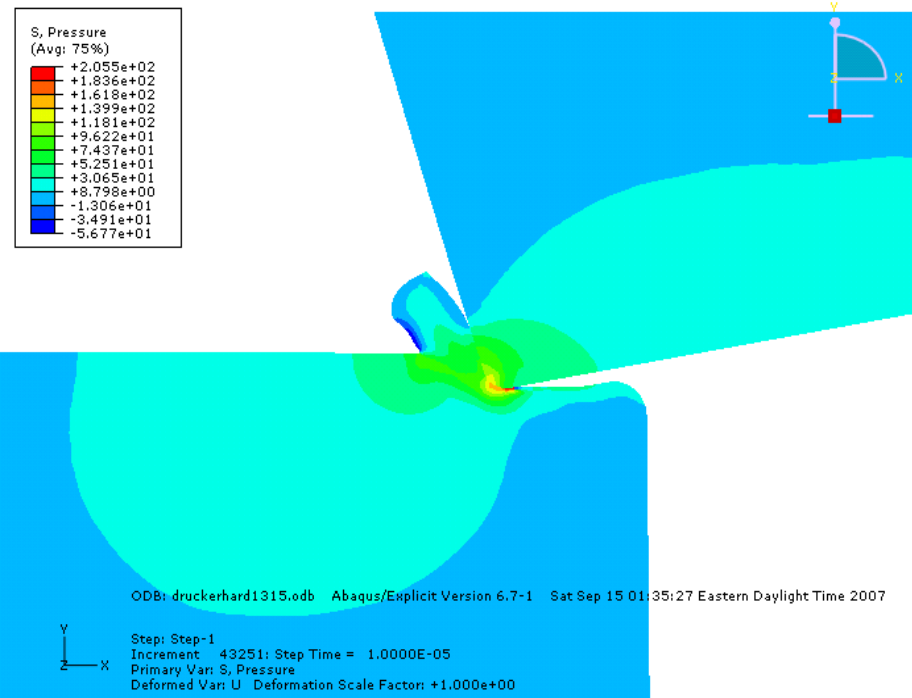
(a)

Elastic modulus, $Nm^{-2}$	$411 \times 10^9$
Density, $kgm^{-3}$	3550
Poisson's ratio	0.16
Initial yield stress, $Nm^{-2}$	$12.5 \times 10^9$
Friction angle, <i>degrees</i>	13
Dilation angle, <i>degrees</i>	-5
K	0.92

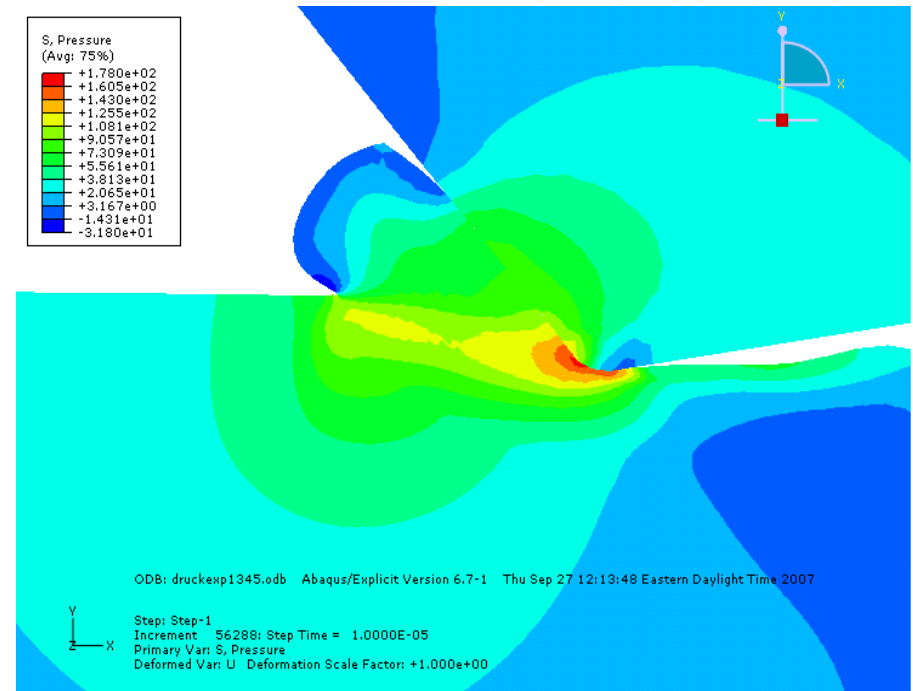
(b)

Material properties of (a) Diamond tool and (b) SiC workpiece

# Parametric studies – Hydrostatic pressure fields with rake angle



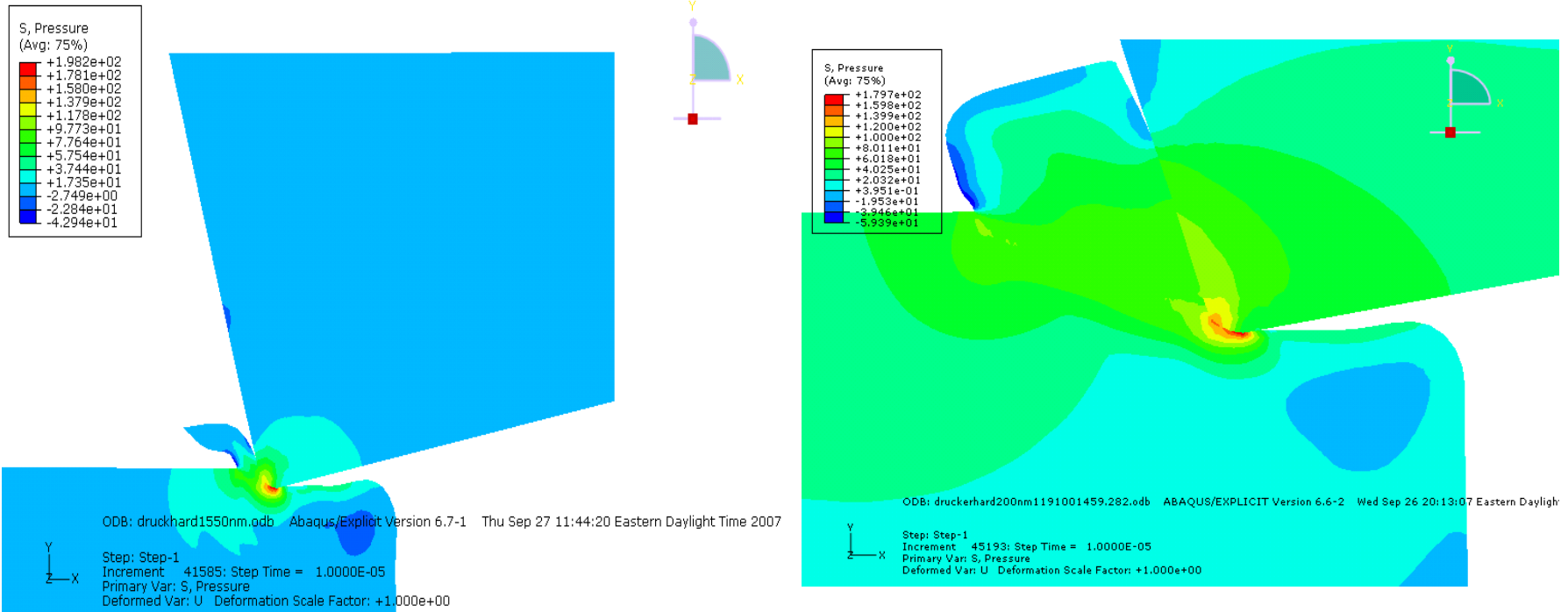
(a)



(b)

Hydrostatic pressure ( $\times 10^8$  Pa) after the end of cut for a rake angle of (a) -  $15^\circ$  and (b)  $-45^\circ$

# Hydrostatic pressure field variation with depth of cut



Hydrostatic pressure ( $\times 10^8$  Pa) for a depth of cut of (a) 50 nm and (b) 200 nm

## Summary – Orthogonal machining simulations of SiC

- Based on the initial results from the simulations of steel, an orthogonal machining model for brittle workpiece materials such as SiC with a single point diamond tool was successfully developed.
- Contour plots obtained from the parametric studies indicate a zone of very high pressure on the order of the hardness of the workpiece material within the primary shear zone.
- From the parametric studies, a definitive relation between rake angles and the maximum generated pressure fields cannot be established.
- The maximum hydrostatic pressure values were greater than the workpiece material hardness throughout the period of cutting which supports the possibility of a ductile regime machining accompanied by High Pressure Phase Transformation (HPPT).
- Also the maximum pressures generated were found to decrease with increase in depth of cut.

# Conclusions from Experiments

- Scratch and edge machining tests on a single crystal SiC helped to identify the critical depth of cut for DBT. After observing the scratches using SEM and AFM Different regions of scratch, i.e., ductile, transition and brittle regions were identified. Entirely ductile machining possible with depths of cuts less than 60 nm.
- Presence of curly chips from the edge machining studies provided strong evidence for a ductile regime machining phenomenon. The diamond tool stayed good for a cutting time of approximately 120 minutes before failing catastrophically. Abrasion was believed to be the predominant mechanism that caused the tool wear and eventual catastrophic failure.
- From the tool wear tests, It was found that the wear mechanism of diamond tools were different for different tool geometries and with different tool manufacturers for the identical cutting conditions. Analyses of machining forces show that the thrust forces dominated the cutting forces throughout the period of cutting for the cutting tests with both radius and straight edged tools. Also analyses of machined workpiece edges had shown that the machining tests with the radius tool produced a better surface finish than the machining tests with the straight edged tool.

# Conclusions from simulations

- For the nano-indentation studies of SiC, a Drucker-Prager material model with negative dilation angle was considered to account for the pressure dependent yield behavior and volume change. The volume changes predicted in the simulations were at the most 5%, which was significantly lower than the 20% (or higher) reduction reported in the literature.
- The predicted values of the hydrostatic pressure were in excess of the hardness value of SiC at the onset of yield, thus indicating that the present model can be adequately used with some modifications to capture the volume reductions more accurately.
- For the orthogonal machining simulations of a steel workpiece, Mises stress and temperature results were found to agree with previous published works from the literature. The simulation results give us a starting point for modeling ductile regime machining of a pressure dependent material such as SiC.
- For the orthogonal machining simulations of SiC workpiece with a diamond tool, contour plots from the parametric studies indicate a zone of very high pressure on the order of the hardness of the workpiece material within the primary shear zone thus supporting the hypothesis of ductile regime machining accompanied by HPPT and shear.

# Future work

- More scratch and edge machining tests need to be done with varying parameters of feed, depth of cut and rake angle to identify suitable conditions for ductile regime machining to occur.
- Ductile regime machining require depths of cuts maintained in the order of tens of nanometers with a high degree of accuracy. Further improvements in process as well as equipment are needed for higher efficiency in the machining process.
- The Drucker-Prager model used in our study can be able to predict volume changes up to 5 %. Appropriate changes need to be made in the model to capture the higher volume changes reported in literature (greater than 20 %).
- Simulations carried out in the present work are in 2-D. The given simulation model can be extended to 3-D for better understanding of the machining process and comparison to experiments.

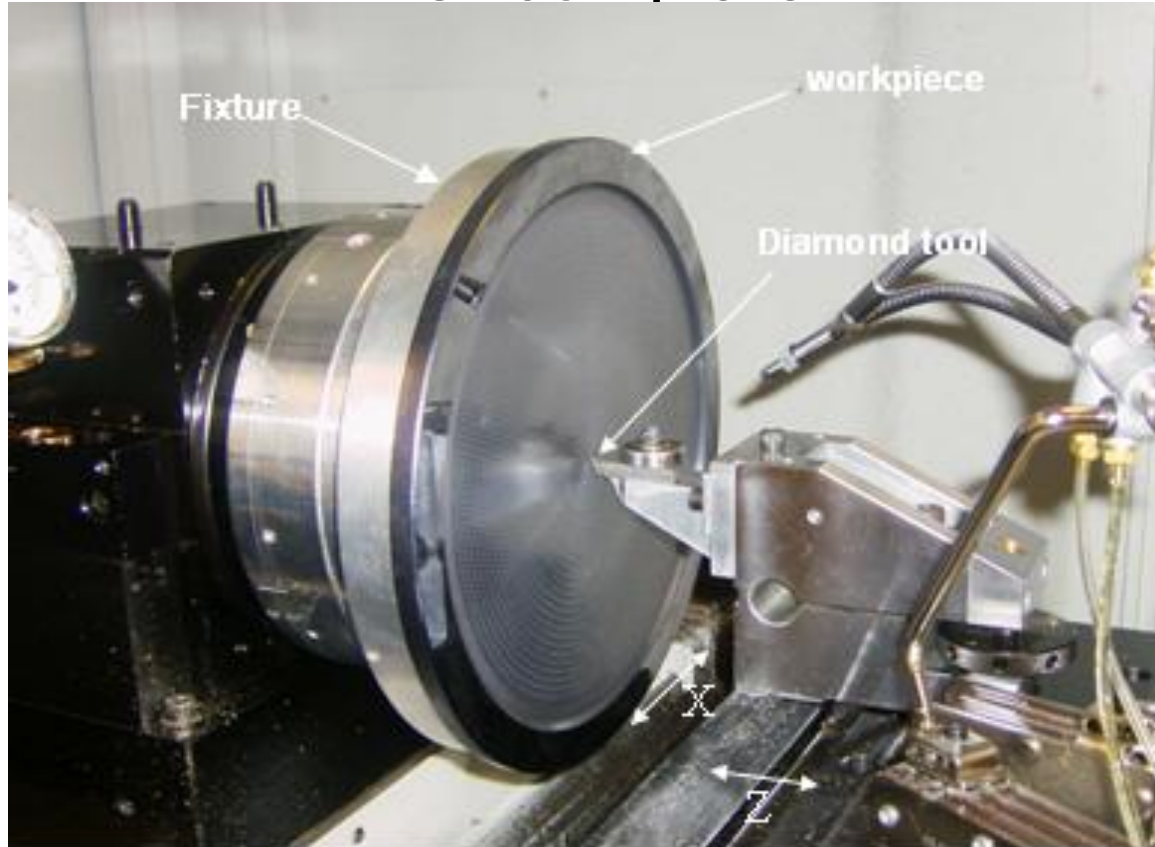
# Acknowledgements

- Dr. Harish Cherukuri and Dr. John Patten.
- Dr. Dave Boyajian, Dr. Ron Smelser and Dr. Kent Curran
- Dr. Kingshuk Bose.
- Center for Precision Metrology.
- DOD/WMU.
- Ronnie Fesperman and Satya Ajjarappu.
- Kannan Subramanian.
- Dr. Peter Blau and Jason Braden (ORNL).
- Dr. Richard Rohrer (NIST).
- Lou Deguzman and Bruce Dudley (Department of Physics, UNCC).

# Questions ?

# Back up

# Face turning experiments on a large single crystal silicon plate



Experimental setup

# Test matrix

<b>Length of cutting</b>	<b>103 mm</b>
<b>Feed</b>	<b>2mm/min</b>
<b>Spindle speed (rpm)</b>	<b>2000</b>
<b>Maximum cutting speed (m/s)</b>	<b>26.6</b>
<b>Cutting fluid</b>	<b>NIST Exp. fluid</b>
<b>Number of cutting tools</b>	<b>2</b>
<b>Tool manufacturer</b>	<b>Edge Tech Inc</b>

(a)

<b>Length of cutting</b>	<b>103 mm</b>
<b>Feed</b>	<b>5mm/min</b>
<b>Depth of cut (<math>\mu\text{m}</math>)</b>	<b>1</b>
<b>Spindle speed (rpm)</b>	<b>2000</b>
<b>Maximum cutting speed (m/s)</b>	<b>26.6</b>
<b>Cutting fluid</b>	<b>NIST Exp. fluid</b>
<b>Number of cutting passes</b>	<b>1</b>

(b)

Machining parameters for cutting tests with (a) radial rake tool and (b) planar rake tool

## Summary – Face turning experiments on a large silicon plate

Tool	Cutting pass	Depth of cut (μm)	Extent of mirror like finish (mm)
1	1	3	40
	2	3	25
	3	3	--
2	1	3	15
	2	1	10
	3	1	--

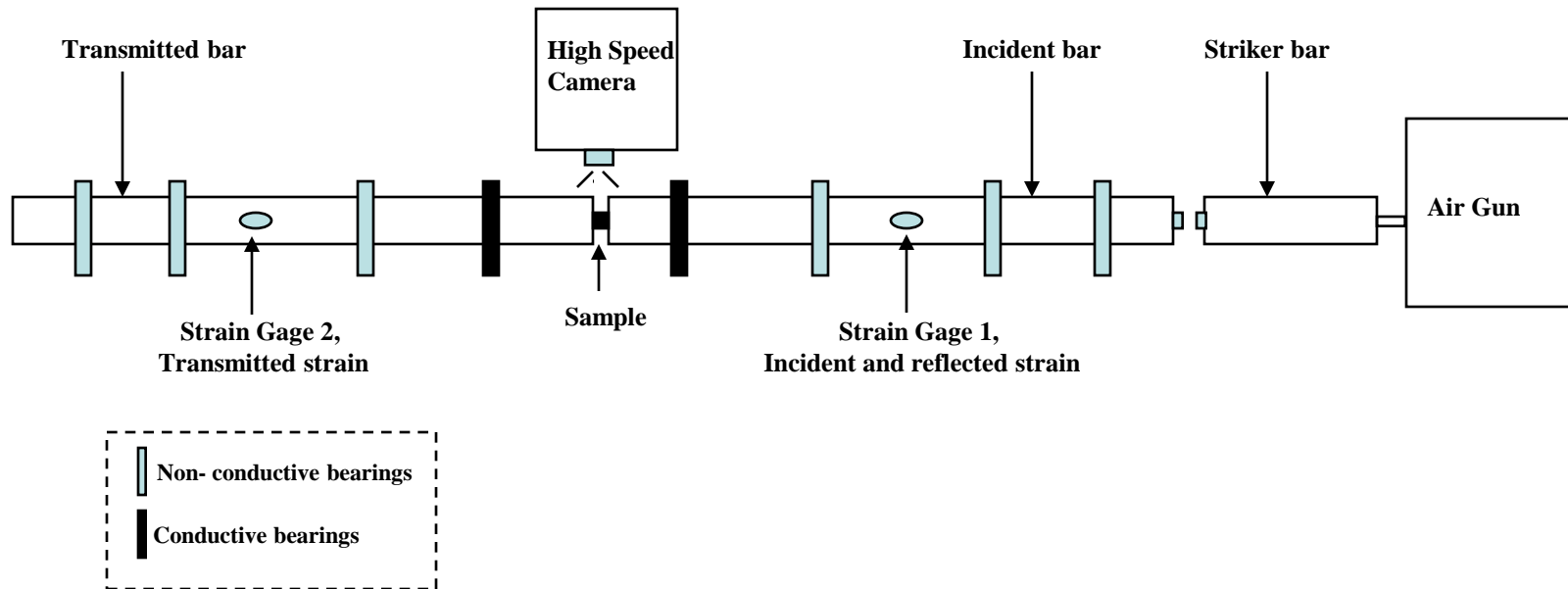
Extent of mirror-like surface for each cutting pass - Face turning experiments with a radial rake tool.

### Key Observations

The extent of mirror-like surface finish was found to be greater for the cutting passes from I.D to the O.D than the cutting passes from O.D to I.D For the experiments with a radial rake tool, no uniform tool wear was observed after the cutting experiments.

For the cutting tests with a planar rake tool, a detailed analyses was not possible due to accidental tool breakage during the course of the tests.

# Split Hopkinson Bar tests on poly-crystalline SiC



Schematic of the SPHB test facility at NIST

Material	Dimension (mm)	
	Length	Diameter
Steel bar (input and transmitted)	1500	15
SiC	4	4

Dimensions of the steel bar and the specimen material

Density (Kg/m <sup>3</sup> )	3250
Flexural Strength (MPa)	480
Elastic Modulus (Gpa)	410
Poisson's Ratio	0.21

Physical properties of SiC specimen material

## Estimation of Failure stress

The Failure stress in the specimen is given by the expression

$$\sigma(t) = \frac{AE\epsilon_t}{A_s}$$

Where  $\sigma(t)$  is the failure stress for the specimen at the given strain rate.

A - cross-sectional area of the steel bar,  $A_s$ - cross-sectional area of the specimen material and E- Young's modulus of the steel bar

All the constants in the above expression are known except  $\epsilon_t$  i. e., the strain in the transmitted bar which is recorded by the strain gage during the tests

Using the given expression and strain gage readings the failure stress of the given SiC material at a high strain rate (  $2 \times 10^3$ ) is obtained as 8. 09 GPa

## Summary – Hopkinson bar tests on polycrystalline SiC

- The fracture stress value of silicon carbide obtained in the tests gave us a starting point for understanding the mechanical behavior of silicon carbide at high strain rates.
- Unlike for metals, there is no standard testing procedure for Kolsky bar testing for ceramic materials such as SiC. Much of the variability is due to experimental errors and variations in testing procedures.
- More tests need to be done for repeatability to determine the exact fracture stress at high strain rates.
- Great care need to be taken to prevent the steel bars from damage when performing tests with hard specimen materials such as SiC.